# Aberrant cohesin function in *Saccharomyces cerevisiae* activates Mcd1 degradation to promote cell lethality

Running title: A cohesin surveillance mechanism

Gurvir Singh[1] and Robert V. Skibbens[1]*.

[1]Department of Biological Sciences, Lehigh University, 111 Research Drive, Bethlehem, Pennsylvania, 18015. United States of America.

* Corresponding author: Robert V. Skibbens, rvs3@lehigh.edu

Key words: Cohesins; Eco1/Ctf7/ESCO2; Rad61/WAPL; Mcd1/Scc1/RAD21; Roberts Syndrome (RBS); Cornelia de Lange Syndrome (CdLS), E3 ligase, San1, Das1, Checkpoints, sister chromatid cohesion, chromosome condensation

# ABSTRACT

The cohesin complex is composed of core ring proteins (Smc1, Smc3 and Mcd1) and associated factors (Pds5, Scc3, and Rad61) that bind via Mcd1. Extrusion (looping from within a single DNA molecule) and cohesion (the tethering together of two different DNA molecules) underlie the many roles that cohesins play in chromosome segregation, gene transcription, DNA repair, chromosome condensation, replication fork progression, and genome organization. While cohesin functions flank the activities of critical cell checkpoints (including spindle assembly and DNA damage checkpoints), the extent to which checkpoints directly target cohesins, in response to aberrant cohesin function, remains unknown. Based on prior evidence that cells mutated for cohesin contain reduced Mcd1 protein, we tested whether loss of Mcd1 is based simply on cohesin instability or integrity. The results show that Mcd1 loss persists even in *rad61* cells, which contain elevated levels of stable chromosome-bound cohesins, and also in *scc2-4*, which do not affect cohesin complex integrity. In fact, re-elevating Mcd1 levels suppresses the temperature-sensitive growth defects of all cohesin alleles tested, revealing that Mcd1 loss is a fundamental mechanism through which cohesins are inactivated to promote cell lethality. Our findings further reveal that cells that exhibit aberrant cohesin function employ E3 ligases (such as San1) to target Mcd1 for degradation. This mechanism of degradation appears unique in that Mcd1 is reduced during S phase, when Mcd1 levels typically peak and despite a dramatic upregulation in *MCD1* transcription. We infer from these latter findings that cells contain a negative feedback mechanism used to maintain Mcd1 homeostasis.

# AUTHOR SUMMARY

Cohesins are central to almost all aspects of DNA regulation (chromosome segregation, gene transcription, DNA repair, chromosome condensation, replication fork progression, and genomic organization). Cohesin also play key roles in cell checkpoints: cohesin mutations activate the spindle assembly checkpoint while double strand DNA breaks can elicit a new round of cohesin establishment. In the current study, we provide evidence for a novel cohesin surveillance system that employs E3 ligases that directly target Mcd1, a core component of the cohesin ring structure, for degradation. We further describe a feedback mechanism through which cells dramatically induce *MCD1* transcription to maintain Mcd1 homeostasis. Finally, we provide evidence that requires the re-evaluation of phenotypes associated with other cohesin gene mutations.

52 # INTRODUCTION

53 The identification of checkpoints has produced significant clinical advances over
54 the last half century (1,2). After the discovery that the tumor suppressor *TP53* gene is
55 mutated in more than 50% of all cancers, advances from both basic science and clinical
56 settings led to new strategies through which p53 can be re-activated, mutated p53
57 degraded, or synthetic lethal mechanisms to eliminate cancer cells (3–7). Similarly,
58 highly proliferative cancer cells are disproportionally sensitive to spindle assembly
59 checkpoint inhibitors, compared to non-tumorigenic cells (8–10). Often, factors that
60 exhibit multiple functions, or reside at the nexus of critical pathways, are monitored by
61 surveillance mechanisms and provide important avenues to improve human health.

62 Cohesins are ATPase protein complexes composed of a core ring (Smc1, Smc3
63 and Mcd1/Scc1, herein Mcd1) and associated factors (Rad61, Pds5 and Scc3/Irr1,
64 herein Scc3) that bind via Mcd1 (11–17). Cohesins are central to almost all aspects of
65 DNA regulation (chromosome segregation, gene transcription, DNA repair, chromosome
66 condensation, replication fork progression, and genomic organization) (11,12,14,18–32).
67 Underlying this complex output of roles are two very distinct cohesin functions: extrusion
68 (looping from within a single DNA molecule) and cohesion (the tethering together of two
69 different DNA molecules) (11,12,21,22,25–27). Mutations in cohesins that affect DNA
70 looping can give rise to severe developmental abnormalities such as Cornelia De Lange
71 Syndrome (CdLS) and Roberts Syndrome (RBS). These multifaceted maladies often
72 include intellectual disabilities, hearing loss, microcephaly, phocomelia and
73 abnormalities in the heart and gastrointestinal tract (33–39). Mutations that impact

tethering give rise to aneuploidy - a hallmark of cancer cells (40–42). Recent evidence indeed suggests that cancer cells rely on elevated cohesin activity for survival (43–47).

It is well established that cohesin functions flank critical cell checkpoints. For instance, cohesin mutations that abolish sister chromatid cohesion (tethering) activate the spindle assembly checkpoint (48–50), consistent with classic micromanipulation and laser ablation studies that cells monitor chromosome biorientation, and thus tension, produced across the two mitotic half-spindles (51–56). In contrast, double strand DNA breaks activate ATM/ATR and CHK1 kinases that elicit a *de novo* round of cohesin deposition and cohesion establishment both at sites of damage and genome-wide (18,24,57–63). The remarkable involvement of cohesins in cell cycle checkpoints, both to maintain euploidy and promote error-free DNA damage repair, underscores their central role in maintaining genome integrity.

In this study, we present evidence that cohesins are a direct target of a surveillance system that may cull aneuploid or transcriptionally aberrant cells from a normal population. The current study was motivated, in part, by prior observations that cohesin mutations result in a significant reduction of Mcd1 protein (64–67). Importantly, the significance of Mcd1 reduction, and mechanisms involved, remained undetermined. Here we show that Mcd1 reduction in cohesin mutant cells is not a benign product of cohesin mutations but significantly contributes to their lethality. Importantly, the loss of Mcd1 occurs independent of defects in either cohesin complex stability or integrity. Finally, we show that cohesin dysfunction activates a surveillance system that employs E3 ligases and the proteasome to specifically target Mcd1 for degradation.

# RESULTS

**Cohesin dysfunction activates a novel mechanism to reduce Mdc1**

The majority of cohesin-mutated cells tested to date (*smc1-259*, *smc3-42*, *pds5-1*, *pds5*Δ *elg1*Δ, and *eco1*Δ *rad61*Δ) contain significantly reduced levels of Mcd1 protein (64–67). Eco1/Ctf7 (herein Eco1) is an acetyltransferase that targets Smc3 to promote stable cohesin-DNA association (48,66,68–71). Rad61 dissociates cohesin from DNA such that *rad61*Δ cells retain elevated levels of stably-bound cohesins (15,72–79). Given the opposing activities of Eco1 (cohesin stabilization,(48,66)) and Rad61 (cohesin dissociation (15)), we hypothesized that *rad61*Δ cells should retain wildtype levels of Mcd1 and suppress the loss of Mcd1 in *eco1* mutated cells. To test these predictions, log phase cultures of wildtype, *rad61*Δ, *eco1-203*, and *eco1*Δ *rad61*Δ cells were arrested in early S phase (hydroxyurea, HU) prior to shifting to 37°C (Fig 1A). Surprisingly, Western blot quantifications of the resulting extracts revealed that Mcd1 levels are reduced not only in *eco1* temperature-sensitive (ts) strains, but also significantly reduced in *rad61*Δ cells (Figs 1B, 1C). Nor did the deletion of *RAD61* provide any benefit to *eco1*Δ cells with respect to Mcd1 levels (Figs 1B, 1C). These results suggest that Mcd1 is reduced by a mechanism that is independent of cohesin complex stability.

Given the results above, it became important to test whether the loss of Mcd1, in the absence of cohesin function, is unique or whether other cohesin complex components are similarly reduced? To address this, we examined Pds5 protein levels in *eco1*Δ *rad61*Δ cells - a factor that relies on Mcd1 for cohesin-association (13,14). As above, log phase cultures of wildtype and *eco1*Δ *rad61*Δ cells were arrested in early S

119 phase (HU) prior to shifting to 37°C. Extracts of the resulting cells were then assessed
120 by Western blot for Pds5 levels. The results indicate that, even though Mcd1 protein is
121 indeed reduced, there is no statistical significance between the level of Pds5 protein
122 across wildtype and *eco1*Δ *rad61*Δ cells (S1 Fig A,B,C). Thus, Mcd1 reduction appears
123 to be a specific feature of cells deficient for cohesin function.

124 The apparent unique reduction of Mcd1 in *eco1*Δ *rad61*Δ, *rad61*Δ, and *eco1-1*
125 cells, all of which retain structurally intact cohesin complexes, is remarkable. It thus
126 became important to further test the extent to which Mcd1 levels might be reduced in
127 cells deficient in Scc2 function. Scc2 is essential for cohesin loading but, as neither a
128 core nor auxiliary component, plays no role in cohesin complex assembly or integrity
129 (80–83). Log phase cultures of wild-type and *scc2-4* cells were arrested in S phase
130 (HU) for 2 hours at 23°C (permissive temperature) and then shifted to 37°C for 1 hour
131 (Fig 2A). Extracts of the resulting cultures were assessed by Western blot to quantify
132 Mcd1 protein levels. The results reveal that Mcd1 is significantly reduced in *scc2-4*
133 mutant cells, compared to wild-type cells (Fig 2B, 2C). We infer from these findings that
134 a novel surveillance system exists that monitors for aberrant cohesin function, rather
135 than cohesin structure, to regulate Mcd1 protein levels.

136

## 137 A negative feedback loop regulates *MCD1* expression

138 The near ubiquitous reduction of Mcd1 in cohesin-mutated cells prompted us to
139 uncover the underlying molecular mechanism. Mcd1 is unique among cohesin subunits
140 in that it is the only core subunit that is degraded at anaphase onset (to allow for sister
141 chromatid segregation), and then transcribed starting at the G1/S transition, each and

every cell cycle (11,66,84). Previous findings documented a complex transcriptional network that regulates *MCD1* expression (65). It thus became important to test the extent to which *MCD1* transcription is reduced in the *eco1*Δ *rad61*Δ cells. Log phase wildtype and *eco1*Δ *rad61*Δ cells were arrested in early S phase (HU) (Fig 3A) - a point in the cell cycle at which *MCD1* expression and Mcd1 protein levels both peak in wildtype cells, but in which Mcd1 protein levels are significantly reduced in *eco1*Δ *rad61*Δ cells (11,65). We confirmed that Mcd1 protein levels were significantly reduced in the same *eco1*Δ *rad61*Δ cultures (Fig 3B, 3C) that we used to test for changes in *MCD1* transcription. In contrast to the model in which *MCD1* transcription is decreased, quantification of qRT-PCR revealed that *MCD1* transcript levels are instead significantly increased (~5.5 fold) in *eco1*Δ *rad61*Δ cells compared to wildtype cells (Fig 3D). These results indicate that the loss of Mcd1 protein in *eco1*Δ *rad61*Δ cells is not dependent on reduced *MCD1* transcription. Moreover, our findings reveal a compensatory feedback mechanism in which cells increase *MCD1* transcription in response to decreased Mcd1 protein levels.

## Identification of an E3 ligase mechanism that promotes Mcd1 degradation

Having excluded a transcription-based mechanism, it became important to test the extent to which the reduction in Mcd1 protein level occurs through degradation. Esp1, a caspase-type protease, cleaves Mcd1 during anaphase onset (65,84–86). If Esp1 cleaves Mcd1 in response to reduced cohesin function, then Mcd1 levels should increase in cells that harbor *ESP1* mutations. To formally test this hypothesis, *eco1*Δ

165 *rad61*Δ cells and *esp1-1* cells were mated and the resulting diploids sporulated and
166 dissected. Log phase cultures of the resulting strains were then tested for changes in
167 temperature-sensitive growth defects. Surprisingly, reduced Esp1 activity failed to
168 suppress *eco1*Δ *rad61*Δ cells ts growth defects and in fact further exacerbated the
169 growth defects (S2 Fig A, B). We further note the 83 kDa and 48 KDa fragments
170 produced by Esp1-dependent degradation of Mcd1 (87,88) are largely absent in our
171 Western blots of cells that harbor cohesin defects (Figs 1B, 2B, 6B). These findings
172 largely negate a scenario in which Esp1 is targeting Mcd1 in response to deficits in
173 cohesin function and further support prior evidence that Esp1 activity is predominantly
174 limited to anaphase onset (84,86).

175 Protein ubiquitination, through E3 ligases, play key roles in numerous cellular
176 activities that include degradation (89,90). Thus, we focused on E3 ligases as a
177 mechanism to reduce Mcd1 protein levels, a model supported evidence that Mcd1 is
178 ubiquitinated (91,92). The E3 ligases that target Mcd1, however, remain unidentified.
179 Thus, we generated *de novo* a candidate list based on genetic or physical interactions
180 reported in either BioGrid or SGD (*Saccharomyces* Genome Database) across the
181 various cohesins subunits (93–96). These efforts resulted in a list of six candidates
182 (Bre1, Bul2, Ldb19, Ubr1, Das1, and San1), all of which are encoded by non-essential
183 genes. These E3 ligases respond to various cell challenges such as oxidative stress
184 (Bre1), heat-shock responses (Bul2), starvation (Ldb19), N-end rule degradation (Ubr1),
185 cell cycle progression (Das1), and nuclear aggregates (San1) (SGD). We reasoned that
186 if any one of the E3 ligases are in part responsible for ubiquitinating Mcd1, then their
187 deletion should suppress *eco1*Δ *rad61*Δ cell ts growth defects. To test this model, each

188 of the E3 ligase genes (*BRE1*, *BUL2*, *LDB19*, *UBR1, DAS1* and *SAN1*) were individually
189 deleted from wildtype and *eco1*Δ *rad61*Δ cells. Log phase cultures of the resulting
190 transformants were serially diluted onto rich medium plates and incubated at either
191 30°C or 37°C, temperatures respectively permissive and non-permissive for *eco1*Δ
192 *rad61*Δ cell growth (Fig 4). Deletion of *BUL2* or *UBR1* had no impact on either wildtype
193 or *eco1*Δ *rad61*Δ cells at either temperature (Fig 4A, 4D). Deletion of *BRE1* exhibited an
194 adverse effect on both wildtype and *eco1*Δ *rad61*Δ cells (Fig 4B), consistent with a prior
195 report that *bre1*Δ cells exhibit genomic instability (97). Compared to the adverse but
196 non-specific impact of *BRE1* deletion, deletion of *LDB19* produced a severe negative
197 impact specific to *eco1*Δ *rad61*Δ cells (Fig 4C). In contrast to the results above, deletion
198 of *SAN1*, and to a lesser extent *DAS1*, suppressed the ts growth defects otherwise
199 exhibited by *eco1*Δ *rad61*Δ cells (Fig 4E, 4F).

200 The findings above suggest that the E3 ligase San1 plays a critical role in Mcd1
201 degradation. If correct, then *eco1*Δ *rad61*Δ cells further deleted of *SAN1* should retain
202 higher levels of Mcd1, compared to *eco1*Δ *rad61*Δ cells. To directly test this prediction,
203 log phase cultures of *eco1*Δ *rad61*Δ cells and *eco1*Δ *rad61*Δ *san1*Δ cells were arrested
204 in S phase (HU) and the resulting extracts assessed by Western blot (Fig 5A, 5B). The
205 results document that Mcd1 protein levels are significantly increased (~36%, based on 3
206 biological replicates) in *eco1*Δ *rad61*Δ cells that are further deleted of *SAN1* (Fig 5C). In
207 summary, our genetic findings that deletion of *SAN1* from *eco1*Δ *rad61*Δ cells partially
208 suppresses the ts phenotype, combined with biochemical studies that *SAN1* absence
209 leads to an increase of Mcd1 levels, provide strong support for the model that cohesin
210 dysfunction activates E3 ubiquitin ligase-mediated degradation of Mcd1. However,

211 because *SAN1* deletion only partially rescues the *eco1*Δ *rad61*Δ phenotype, additional
212 E3 ligases involved in Mcd1 turnover are likely involved.
213

## 214 The proteasome degrades Mcd1 in *eco1 rad61* cells during mitosis

215 The above findings are noteworthy both for documenting reduced Mcd1 levels
216 during S phase (when Mcd1 protein and *MCD1* expression levels peak during the cell
217 cycle) and for the identification of an E3 ligase pathway that targets Mcd1 for
218 degradation. Together, these results raise the possibility that cells respond to cohesin
219 dysfunction by promoting Mcd1 degradation via the proteosome, potentially in a cell
220 cycle manner. To test this prediction, *PDR5*, which encodes a drug efflux pump, was
221 deleted in *eco1*Δ *rad61*Δ cells to allow for the retention of MG-132 - a proteasome
222 inhibitor (98). We first tested whether proteosome inhibition might result in the retention
223 of Mcd1 during S phase. Log phase cultures of *eco1*Δ *rad61*Δ *pdr5*Δ triple mutant cells
224 were arrested in S phase for 2 hours, followed by treatment with MG-132 or DMSO
225 (control) in the presence of hydroxyurea (S3 Fig A). Remarkably, changes in Mcd1
226 protein levels remained similar across cells incubated in either DMSO or MG-132 (S3
227 Fig B,C), suggesting that Mcd1 degradation occurred elsewhere in the cell cycle. Since
228 Mcd1 is essential during M phase, and minimally produced in G1 (11), we assessed the
229 extent to which Mcd1 degradation occurs prior to anaphase onset. Log phase cultures
230 of *eco1*Δ *rad61*Δ *pdr5*Δ triple mutant cells were incubated in media that contains
231 nocodazole (to synchronize cells preanaphase) along with either MG-132 (proteosome
232 inhibitor) or a DMSO control. The progression of cells from log-phase growth to a pre-
233 anaphase arrest was monitored by flow cytometry (Fig 6A). Extracts of the resulting

234 cultures were then assessed by Western blot (Fig 6B). Quantification of the resulting
235 blots reveal that Mcd1 levels are significantly elevated (nearly 3 fold) in cells incubated
236 in the presence of MG-132, compared to the DMSO control (Fig 6C). Together, these
237 results reveal that degradation occurs prior to anapahase onset, when Mcd1 is essential
238 for sister chromatid cohesion, through a post-ubiquitination process performed by the
239 proteosome. The extent to which Mcd1 is similarly degraded in G1 or G2 phases
240 remains to be determined in future studies.
241

## 242 *MCD1* overexpression rescues the inviabilty of cohesin mutated cells

243 The reduction in Mcd1 protein levels is an attribute common to all cohesin
244 mutated cells tested to date (64–67, current study). This near ubiquitous reduction
245 prompted us to ask the following question: are ts growth defects due to the mutated
246 cohesin alleles (ie. Mcd1 loss is a downstream consequence of cohesin inactivation, but
247 otherwise unimportant) or due to the reduction in Mcd1? To differentiate between these
248 two possibilities, we tested the extent to which elevated expression of *MCD1* could
249 suppress the lethality of cells that harbor ts mutations in other cohesin genes. Wildtype,
250 *eco1-1*, *scc3-6*, *smc3-42*, and *smc1-259* cells were each transformed with either vector
251 alone or vector that drives elevated expression of *MCD1*. Log phase cultures of the
252 resulting transformants were then serially diluted onto selective media plates and
253 incubated across a range of temperatures. As expected, elevated *MCD1* expression
254 had no effect on the growth of wildtype cells at the temperatures tested. In contrast,
255 overexpression of *MCD1* suppressed the ts growth defects in all five cohesin ts alleles
256 (Fig 7) - in some cases up to 37°C. We further found that elevated *MCD1* expression

257 suppressed the ts growth defect of *scc2-4* mutant cells, cells that contain wildtype
258 alleles of each cohesin gene subunit (Fig 7E). Importantly, the suppression of growth
259 defects is unique to *MCD1*: overexpression of *ECO1* failed to rescue the ts growth
260 defects of *smc3-42*, *smc1-259*, *mcd1-73*, and *pds5-3* cells (99) and overexpression of
261 *PDS5* failed to rescue the ts growth defects of *eco1*Δ *rad61*Δ (Fig S1D). Nor did the
262 deletion of *RAD61* (which is required for *eco1*Δ cell viability (70,73,100)), rescue the
263 viability of *smc3-42* or *mcd1-1* mutant strains (101). These results provide evidence that
264 the targeted loss of Mcd1 significantly contributes to the lethality of cohesin-mutated
265 cells, and also confound prior interpretations of the severity of phenotypes attributed
266 solely to those ts alleles.
267

268 **Loss of Mcd1 differentially impacts cohesion and condensation**

269 Above, we established loss of Mcd1 as a key driver of most, if not all, cohesin-
270 mutated strain lethalities. It next became important to test the extent to which Mcd1 loss
271 exacerbated cohesin functions. Wildtype and *smc1-259* strains were genetically
272 modified to contain either an rDNA condensation marker (Net1-GFP) or a cohesion
273 assay cassette (tetO and TetR-GFP) (11,12,14,76,78,102,103). The modified strains
274 were then transformed with a high-copy vector alone or vector that drives elevated
275 expression of *MCD1*. Log phase cultures of the resulting transformants were arrested in
276 G1 (alpha factor, αF) and then released into 34°C (non-permissive for *smc1-259* cells)
277 rich medium that contains nocodazole (NZ) to arrest cells in preanaphase. DNA content
278 (flow cytometry) and cell morphologies were monitored at various stages of both
279 experiments (Figs 8A, 9A).

280 Notably, *smc1-259* mutant cells have not been previously assessed for
281 condensation defects. Here, we exploited the well-established analysis of rDNA
282 chromatin architecture using Ne1-GFP (11,14,76,78,104). In wildtype cells, rDNA
283 converts from a decondensed puff-like structure during G1 into tight loops (occasionally
284 observed as bars) during mitosis (105). As expected, wildtype cells arrested in
285 preanaphase exhibited well-defined rDNA loops, indicative of robust chromosome
286 condensation (Fig 8B, 8C). In contrast, only 21% of *smc1-259* cells contained tight
287 loops such that the majority of cells exhibited defects in rDNA condensation (Fig 8B,
288 8C). These results extend prior findings regarding the condensation defects exhibited by
289 other cohesin mutated strains (11,32,48,75,101,106,107). Elevated expression of *MCD1*
290 had no observable impact on rDNA structure in wildtype cells. Surprisingly, *MCD1*
291 expression produced only a modest increase (38%, compared to 21% in the vector
292 control) in the percent of *smc1-259* cells that contained condensed rDNA loops (Fig 8C).
293 Given prior evidence that suppression of condensation defects underlies the improved
294 viability of cohesin-mutated cells (108), we decided to further investigate the
295 condensation of rDNA structure. Mutated cells that did not contain tight and well-defined
296 rDNA loops were parsed into two categories: puff-like (fully decondensed) and in which
297 some structure was apparent within the rDNA mass (partial decondensation). Focusing
298 on the more severe of the two phenotypes, *smc1-259* cells that contained vector alone
299 were strongly biased toward the frequency of puffs (~65% puffs compared to 12%
300 partial condensed) (Fig 8D, S4 Fig). *smc1-259* cells in which *MCD1* was over
301 expressed, however, contained a significant decrease in the frequency of puffs (25%,
302 down from 65% for vector alone) (Fig 8D). In combination, these findings reveal that the

303 loss of Mcd1 significantly contributes to the condensation defects that might otherwise
304 be attributed to the *smc1-259* allele.
305 Next, we assessed the effect of reduced Mcd1 on sister chromatid cohesion. In
306 wildtype cells, the combination of GFP-tetR/tetO, which marks each sister chromatid,
307 document close tethering such that both loci appear as a single dot. In cohesin mutated
308 cells, separated sisters are readily detected as two dots (12). Elevated expression of
309 *MCD1* in wildtype cells resulted in normal frequencies of tethered sister chromatids (1
310 dot/nucleus), similar to vector alone (Fig 9 B,C). *smc1-259* cells that contained vector
311 alone exhibited a high (60%) frequency of 2 dots/nucleus (Fig 9 B,C), consistent with
312 prior studies and the frequency of cohesion defects observed in other cohesin mutated
313 cells (11,48,80,101,106,108). Notably, elevated expression of *MCD1* significantly
314 restored sister chromatid tethering in *smc1-259* cells, with only 35% (compared to 60%
315 vector control) of cells exhibiting cohesion defects. In combination, the above findings
316 reveal a surprisingly biased role for Mcd1 in promoting cohesion with a more nuanced
317 role in promoting chromosome condensation.
318

319 # DISCUSSION

320 The cohesin component Mcd1, which caps the ATPase domains of Smc1 and
321 Smc3 to form the core cohesin complex, is greatly reduced in cells that harbor
322 mutations in nearly every cohesin gene tested to date (64–67). A priori, a simple
323 explanation is that cohesin gene mutations destabilize the cohesin ring and, in some
324 unknown fashion, promote the loss of the non-mutated Mcd1 protein. The first revelation
325 of the current study is that Mcd1 levels are also significantly reduced in cells mutated for

326 regulatory mechanisms in which the cohesin complexes remain intact. For example,
327 cells that are fully absent of *ECO1* and *RAD61* cells exhibit reduced Mcd1. Strikingly,
328 Mcd1 is significantly reduced even in *rad61*Δ cells in which cohesins appear hyper-
329 stabilized, exhibit extended DNA-associations, and are fully functional to condense
330 chromosomes and extrude DNA loops (15,65,72,73,75–79,109,109). Mcd1 is also
331 reduced in *scc2-4* cells, which exhibit cohesin loading defects, but have no known
332 defect in either cohesin complex assembly or integrity (80–83). These findings, coupled
333 with the recognition that it is wildtype Mcd1 protein that is reduced, not a mutated
334 version, are inconsistent with a simple instability or integrity model. Intriguingly,
335 reduction of RAD21, the human ortholog of Mcd1, appears to be a conserved feature of
336 cells that harbor cohesin gene mutations (110–114), but the significance of either Mcd1
337 or RAD21 reduction remained largely unrecognized. In summary, our current study
338 suggests that cohesin function is strongly regulated through Mcd1/RAD21 stability, and
339 that manipulating its levels may have significant implications in cohesinopatheis and
340 cancer research.

341 The second set of findings reported here impact all prior analyses of cohesin
342 mutated strains. Previously, phenotypes exhibited by mutated cohesin strains were
343 interpreted to reflect protein inactivation/misfolding of the particular gene under study.
344 Instead, we find substantial suppression of the ts growth defects that occur in cohesin
345 mutated cells (*smc1-259*, *smc3-42*, *scc3-6*, *scc2-4* and *eco1*$^{ctf7\text{-}203}$) simply by re-
346 elevating Mcd1 levels. Moreover, our results differentiate Mcd1 roles in cohesion and
347 condensation: re-elevating Mcd1 levels produced an overtly increased suppression of
348 cohesin defects, compared to condensation defects, in *smc1-259* cells. We infer from

349 these findings two key principles. First, that Mcd1-dependent restoration of cohesion
350 (and to a lesser extent condensation) primarily accounts for the decrease in
351 temperature-sensitive growth of *smc1-259* cells. Second, that Smc1 appears to exert a
352 more significant role in condensation (and possibly less a significant role in cohesion)
353 than previously reported. In combination, these findings suggest that a re-evaluation of
354 phenotypic severity, previously attributed to cohesin gene mutations, is warranted. More
355 broadly, studies that characterize phenotypes for a mutated component within a
356 complex should be coupled with analyses regarding the persistence of the remaining
357 subunits.

358 The third set of findings that emerge from the current study is the identification of
359 the pathway through which Mcd1 is degraded. In unperturbed cells, Mcd1 is degraded
360 at anaphase onset by APC-dependent activation of Esp1 (86,115–117). Here, our
361 findings largely negate a role for an Esp1-dependent mechanism and instead document
362 for the first time that E3 ligases (San1 and Das1) and the proteosome perform
363 unanticipated roles in Mcd1 degradation. Importantly, Mcd1 levels are significantly
364 decreased in both S and M phases in response to cohesin dysfunction. While the
365 proteosome plays a key role in Mcd1 degradation during mitosis (preanaphase onset),
366 proteosome inhibition failed to restore Mcd1 levels during S phase despite roughly a 5-
367 fold increase in *MCD1* transcription. These findings expose a critical gap in knowledge
368 regarding the cell cycle phase of E3 ligase activation that is required to reduce Mcd1
369 during S phase. Moreover, the E3 ligase responsible for Mcd1/RAD21 degradation
370 remain largely unidentified. Future studies aimed at defining this regulatory layer will not
371 only advance our understanding of cohesin regulation but may also provide means to

372 modulate cohesin function through Mcd1 stability, offering new avenues for cohesin-
373 targeted cancer therapies.

374 Another revelation of the current study relates to the mechanism through which
375 yeast cells appear to achieve homeostatic levels of Mcd1. Subsequent to degradation at
376 anaphase onset, cells initiate a new round of *MCD1* transcription at the G1/S transition
377 that results in Mcd1 protein levels that peak during S phase (11). Our results suggest
378 that Mcd1 protein may negatively regulate its own expression such that E3-ligase
379 degradation of Mcd1 (in response to cohesin deficiency) results in a dramatic
380 upregulation in *MCD1* expression during S phase that is well above that of wildtype
381 cells. Given reduced Mcd1 levels exhibited by cohesin-defective cells, degradation
382 appears to be heavily favored over the increase (~5-fold) in transcription, suggesting
383 that the E3 ligases that promote Mcd1 degradation are likely significantly upregulated.

384 The identification of surveillance mechanisms that target Mcd1/RAD21 may
385 significantly impact studies of both human development and cancer progression.
386 However, a limitation of the current study is the lack of a molecular description of how
387 cells detect cohesin dysfunction and, in response, activate Mcd1 degradation. Of
388 several possibilities, cohesion defects that result in the retention of an activated spindle
389 assembly checkpoint may promote the targeting of Mcd1 in mitotic cells or cells that
390 progress into G1. Another possibility is that cohesin-dependent transcriptional defects
391 impact the expression of any number of genes, for example those that encode for Mcd1,
392 E3 ligase inhibitors, or factors that promote cohesin function. More recent evidence
393 suggests that cyclin-dependent kinases (CDKs) also play a critical role in Mcd1
394 regulation. For instance, deletion of the G1 cyclin, *CLN2*, rescues both *eco1Δ rad61Δ*

395 cell ts growth defects and *pds5Δ elg1Δ* lethality - in both cases by increasing Mcd1
396 levels (64,77). These findings raise additional possibilities, including that 1) Cln2-CDK
397 modifies cohesin directly in order to recruit E3 ligases to Mcd1, 2) Cln2-CDK
398 targets/activates E3 ligases (such as San1) to degrade Mcd1, or 3) cohesin represses
399 in some manner the transcription of *CLN2* that otherwise acts to limit *MCD1*
400 transcription. Exploring the pathways through which signals, that arise from cohesin
401 defects, are relayed to E3 ligases constitutes the next important advancement in our
402 understanding of cohesin biology.
403 Finally, Mcd1 targeting appears to extend beyond cells that exhibit cohesin
404 defects. For instance, exposing cells to reactive oxygen species also triggers Mcd1
405 degradation via an apoptotic pathway (118–121). The conserved nature of a
406 surveillance mechanism that targets Mcd1 is supported by findings that RAD21
407 (homolog of Mcd1) is degraded by caspases 3 and 7 during apoptotic responses
408 (118,122,123). Together, these results suggest that inactivating cohesin functions
409 through Mcd1/RAD21 degradation (through E3 ligases or caspases) may represent an
410 evolutionarily conserved mechanism for promoting cell death. Conversely, cells that
411 evade this surveillance system may obtain proliferative benefits. In support of this
412 model, elevated expression of almost every cohesin subunit (RAD21, SMC1A, SMC3,
413 STAG1, PDS5, WAPL) and cohesin regulator (NIPBL, MAU2) appears to be oncogenic
414 and present in a wide range of cancer cells (44,45,47). In fact, 30 of 33 different cancer
415 types were recently shown to express elevated levels of ESCO2 (46). RAD21, however,
416 is the most frequently amplified cohesin in non-small-cell lung cancer, breast cancer
417 cells, cervical cancer, ovarian cancer, oral cancer and prostate cancer (40,124–131).

418 How cancer cells circumvent the transcriptional and degradational mechanisms that
419 normally regulate RAD21 levels remains unclear, but reducing RAD21 levels in cancer
420 cells appears effective in reducing cell proliferation and/or inducing apoptosis
421 (124,125,130,131). These findings, in combination with our current study, highlight the
422 potential for targeting Mcd1, the master regulator of cohesin function, as a novel
423 therapeutic strategy across multiple cancer types.
424

# 425 MATERIALS AND METHODS

426 **Yeast strains, media, and growth conditions**: All strains (see S1 Table for
427 strain genotypes) were grown on YPD-rich media unless placed on selective medium to
428 facilitate plasmid transformation/retention or spore identification (132). Cells that
429 required inhibition of the proteasome, were treated with 75μM MG-132
430 (MedChemExpress Cat No. HY-13259) and a control of DMSO.
431 **Strain generation**: Primers used to delete genes (*BUL2*, *BRE1*, *LDB19*, *DAS1*
432 and *SAN1*) and verify proper integration are listed in S2 Table. GFP-tagging Net1, to
433 include either *kanMX6* or *TRP1* markers, are previously described (133). The cohesion
434 assay strains used in this study (YGS333, YGS334, YGS321, YGS323) were generated
435 by crossing *smc1-259* (YBS3168/ K6013) with wildtype cells that harbor the cohesion
436 assay cassette (*tetO:URA3 tetR-GFP:LEU2 Pds1-Myc:TRP1*) (YBS1042) (103,134).
437 The resulting diploid (YGS301) was sporulated and dissected to obtain *smc1-259*
438 *tetO:URA3 tetR-GFP:LEU2* cells and wildtype cassette strain *tetO:URA3 tetR-*
439 *GFP:LEU2*.

440 Wildtype and cohesin mutant cells overexpressing vector were transformed with
441 either pRS424 plasmid (2μ *TRP1*) or pRS425 (2μ *LEU*) and cells overexpressing *MCD1*
442 were transformed either with pRS425 (2μ *LEU*) or pGS35 (2μ *LEU2 MCD1*) (65). See
443 S1 Table for resulting strain names and genotypes.

444 **Western Blots**: Cell numbers for each log phase strain were normalized to 2
445 $OD_{600}$. Whole cell protein extracts were prepared as described in (135) with minor
446 modifications. Cells were mechanically lysed (Bead-beater, BioSpec) in 17% TCA with
447 regular intermittent cooling on ice. The beads were washed two times in 500μL of 5%
448 TCA and the two lysates combined and centrifuged at 15,000 rpm for 20 min at 4°C with
449 subsequent solubilization in 3% SDS and 0.25 M Tris-base buffer. Western blotting and
450 protein detection using the anti-Mcd1 and anti-Pds5 antibodies (generous gift from Dr.
451 Vincent Guacci and the lab of Doug Koshland), anti-PGK1 (Invitrogen), Goat anti-Mouse
452 HRP (BIO-RAD) or Goat anti-Rabbit HRP (BIO-RAD), were performed as previously
453 described (65). Protein band intensities (obtained by ChemiDoc MP) were quantified
454 using Image J. Significance was determined by a two-tailed test as described in
455 legends.

456 **RNA extraction and qRT-PCR:** Cell numbers from log phase cultures were
457 normalized to 2 $OD_{600}$ , pelleted by centrifugation and frozen in liquid nitrogen. Cells
458 were lysed mechanically using a bead-beater (BioSpec) for 8 min with intermittent
459 cooling on ice. RNA was extracted and purified using the RNeasy Mini Kit (Qiagen) per
460 manufacturer's instructions and quantified using a nanodrop (Thermo Scientific,
461 NanoDrop One$^{C}$). Normalized RNAs were treated with Turbo DNase (Ambion) and then
462 reverse transcribed using SupercriptIII (Invitrogen). Quantitative Real -Time (qRT) PCR

463 was performed in triplicates using the Rotor-Gene SYBR Green PCR kit (Cat. No.
464 204074) and $C_T$ values measured using the Rotor Gene (Corbett). $C_T$ values of *MCD1*
465 and internal control ALG9 were averaged and the fold change in *MCD1* expression
466 determined using the $2^{-\Delta\Delta Ct}$method (136).

467 **Condensation and Cohesion Assays**: Cohesion and condensation assays
468 were performed as previously described (102) with the following modifications. Log
469 phase cells were grown in selective media, followed by pre-synchronized in G1 (alpha
470 factor) for 3 hr at 23°C in YPD- rich media. The resulting cultures were harvested,
471 washed 2 times and then shifted to 37°C for 3 hr in fresh media supplemented with
472 nocodazole. Cell aliquots of the resulting preanaphase arrested cells were fixed at room
473 temperature in paraformaldehyde to a final concentration of 3.7%. Cells were assayed
474 using an E800 light microscope (Nikon) equipped with a cooled CD camera
475 (Coolsnapfx, Photometrics) and imaging software (IPLab, Scanalytics).

476 **Flow Cytometry and Cell Cycle Progression**: Log phase cultures were
477 normalized ($OD_{600}$) and synchronized at specific cell stages using the following
478 treatments: early S phase with 0.2 M Hydroxyurea (SIGMA, H8627), G1 phase with 3
479 μM alpha factor (ZYMO RESEARCH, Y1001), M phase with 20 μg/ml of nocodazole
480 (SIGMA, M1404). Log phase growth and proper cell cycle arrest were confirmed by flow
481 cytometry as previously described (102,109).

482

483 # ACKNOWLEDGEMENTS

484 The authors gratefully acknowledge the generous gifts of Mcd1-directed and
485 Pds5-directed antibodies, as well as numerous yeast strains from Dr. Vincent Guacci

and the Koshland Lab. The authors also thank Skibbens lab members and participants in the Super Group Yeast Club for helpful discussions during the preparation of this paper.

# Financial Disclosure

This work was supported by the National Institutes of Health (R15GM139097) to RVS. The funders had no role in the study design, data collection and analysis, decision to publish, or preparation of the manuscript.

# REFERENCES

1. Hartwell LH, Weinert TA. Checkpoints: Controls That Ensure the Order of Cell Cycle Events. Science. 1989 Nov 3;246(4930):629–34.

2. Uzbekov R, Prigent C. A Journey through Time on the Discovery of Cell Cycle Regulation. Cells. 2022 Feb 17;11(4):704.

3. Masutani M, Nozaki T, Wakabayashi K, Sugimura T. Role of poly(ADP-ribose) polymerase in cell-cycle checkpoint mechanisms following γ-irradiation. Biochimie. 1995;77(6):462–5.

4. Tsukamoto S. Natural products that target p53 for cancer therapy. J Nat Med. 2025 July;79(4):725–37.

5. Nishikawa S, Iwakuma T. Drugs Targeting p53 Mutations with FDA Approval and in Clinical Trials. Cancers. 2023 Jan 9;15(2):429.

6. Li W, Wang F, Guo R, Bian Z, Song Y. Targeting macrophages in hematological malignancies: recent advances and future directions. J Hematol Oncol [Internet]. 2022 Aug 17 [cited 2025 July 15];15(1). Available from: https://jhoonline.biomedcentral.com/articles/10.1186/s13045-022-01328-x

7. Baliakas P, Soussi T. The TP53 tumor suppressor gene: From molecular biology to clinical investigations. J Intern Med. 2025 Aug;298(2):78–96.

8. Weaver BAA, Cleveland DW. Decoding the links between mitosis, cancer, and chemotherapy: The mitotic checkpoint, adaptation, and cell death. Cancer Cell. 2005 July;8(1):7–12.

9. Tanaka K, Hirota T. Chromosome segregation machinery and cancer. Cancer Science. 2009 July;100(7):1158–65.

516 10. Gallego-Jara J, Lozano-Terol G, Sola-Martínez RA, Cánovas-Díaz M, De Diego Puente T.
517 A Compressive Review about Taxol®: History and Future Challenges. Molecules. 2020
518 Dec 17;25(24):5986.

519 11. Guacci V, Koshland D, Strunnikov A. A Direct Link between Sister Chromatid Cohesion and
520 Chromosome Condensation Revealed through the Analysis of MCD1 in S. cerevisiae. Cell.
521 1997 Oct;91(1):47–57.

522 12. Michaelis C, Ciosk R, Nasmyth K. Cohesins: Chromosomal Proteins that Prevent
523 Premature Separation of Sister Chromatids. Cell. 1997 Oct;91(1):35–45.

524 13. Panizza S, Tanaka T, Hochwagen A, Eisenhaber F, Nasmyth K. Pds5 cooperates with
525 cohesin in maintaining sister chromatid cohesion. Current Biology. 2000 Dec;10(24):1557–
526 64.

527 14. Hartman T, Stead K, Koshland D, Guacci V. Pds5p Is an Essential Chromosomal Protein
528 Required for Both Sister Chromatid Cohesion and Condensation in *Saccharomyces*
529 *cerevisiae*. The Journal of Cell Biology. 2000 Oct 30;151(3):613–26.

530 15. Kueng S, Hegemann B, Peters BH, Lipp JJ, Schleiffer A, Mechtler K, et al. Wapl Controls
531 the Dynamic Association of Cohesin with Chromatin. Cell. 2006 Dec;127(5):955–67.

532 16. Game JC, Birrell GW, Brown JA, Shibata T, Baccari C, Chu AM, et al. Use of a Genome-
533 Wide Approach to Identify New Genes that Control Resistance of Saccharomyces
534 cerevisiae to Ionizing Radiation. Radiation Research. 2003 July;160(1):14–24.

535 17. Kurlandzka A, Rytka J, Różalska B, Wysocka M. Saccharomyces cerevisiae IRR1 protein
536 is indirectly involved in colony formation. Yeast. 1999 Jan 15;15(1):23–33.

537 18. Sjögren C, Nasmyth K. Sister chromatid cohesion is required for postreplicative double-
538 strand break repair in Saccharomyces cerevisiae. Current Biology. 2001 June;11(12):991–
539 5.

540 19. Jessberger R. The many functions of smc proteins in chromosome dynamics. Nat Rev Mol
541 Cell Biol. 2002 Oct 1;3(10):767–78.

542 20. Kim JS, Krasieva TB, LaMorte V, Taylor AMR, Yokomori K. Specific Recruitment of Human
543 Cohesin to Laser-induced DNA Damage. Journal of Biological Chemistry. 2002
544 Nov;277(47):45149–53.

545 21. de Wit E, Vos ESM, Holwerda SJB, Valdes-Quezada C, Verstegen MJAM, Teunissen H, et
546 al. CTCF Binding Polarity Determines Chromatin Looping. Molecular Cell. 2015
547 Nov;60(4):676–84.

548 22. Davidson IF, Goetz D, Zaczek MP, Molodtsov MI, Huis In 'T Veld PJ, Weissmann F, et al.
549 Rapid movement and transcriptional re-localization of human cohesin on DNA. The EMBO
550 Journal. 2016 Dec 15;35(24):2671–85.

551 23. Terret ME, Sherwood R, Rahman S, Qin J, Jallepalli PV. Cohesin acetylation speeds the
552 replication fork. Nature. 2009 Nov;462(7270):231–4.

24. Ünal E, Heidinger-Pauli JM, Koshland D. DNA Double-Strand Breaks Trigger Genome-Wide Sister-Chromatid Cohesion Through Eco1 (Ctf7). Science. 2007 July 13;317(5835):245–8.

25. Haarhuis JHI, Van Der Weide RH, Blomen VA, Yáñez-Cuna JO, Amendola M, Van Ruiten MS, et al. The Cohesin Release Factor WAPL Restricts Chromatin Loop Extension. Cell. 2017 May;169(4):693-707.e14.

26. Rao SSP, Huang SC, Glenn St Hilaire B, Engreitz JM, Perez EM, Kieffer-Kwon KR, et al. Cohesin Loss Eliminates All Loop Domains. Cell. 2017 Oct;171(2):305-320.e24.

27. Wutz G, Várnai C, Nagasaka K, Cisneros DA, Stocsits RR, Tang W, et al. Topologically associating domains and chromatin loops depend on cohesin and are regulated by CTCF, WAPL, and PDS5 proteins. The EMBO Journal. 2017 Dec 15;36(24):3573–99.

28. Lara-Pezzi E, Pezzi N, Prieto I, Barthelemy I, Carreiro C, Martínez A, et al. Evidence of a Transcriptional Co-activator Function of Cohesin STAG/SA/Scc3. Journal of Biological Chemistry. 2004 Feb;279(8):6553–9.

29. Rollins RA, Morcillo P, Dorsett D. Nipped-B, a Drosophila Homologue of Chromosomal Adherins, Participates in Activation by Remote Enhancers in the cut and Ultrabithorax Genes. Genetics. 1999 June 1;152(2):577–93.

30. Rollins RA, Korom M, Aulner N, Martens A, Dorsett D. *Drosophila* Nipped-B Protein Supports Sister Chromatid Cohesion and Opposes the Stromalin/Scc3 Cohesion Factor To Facilitate Long-Range Activation of the *cut* Gene. Molecular and Cellular Biology. 2004 Apr 1;24(8):3100–11.

31. Skibbens RV, Marzillier J, Eastman L. Cohesins coordinate gene transcriptions of related function within*Saccharomyces cerevisiae*. Cell Cycle. 2010 Apr 15;9(8):1601–6.

32. Gard S, Light W, Xiong B, Bose T, McNairn AJ, Harris B, et al. Cohesinopathy mutations disrupt the subnuclear organization of chromatin. Journal of Cell Biology. 2009 Nov 16;187(4):455–62.

33. Krantz ID, McCallum J, DeScipio C, Kaur M, Gillis LA, Yaeger D, et al. Cornelia de Lange syndrome is caused by mutations in NIPBL, the human homolog of Drosophila melanogaster Nipped-B. Nat Genet. 2004 June;36(6):631–5.

34. Tonkin ET, Wang TJ, Lisgo S, Bamshad MJ, Strachan T. NIPBL, encoding a homolog of fungal Scc2-type sister chromatid cohesion proteins and fly Nipped-B, is mutated in Cornelia de Lange syndrome. Nat Genet. 2004 June;36(6):636–41.

35. Schüle B, Oviedo A, Johnston K, Pai S, Francke U. Inactivating Mutations in ESCO2 Cause SC Phocomelia and Roberts Syndrome: No Phenotype-Genotype Correlation. The American Journal of Human Genetics. 2005 Dec;77(6):1117–28.

36. Vega H, Waisfisz Q, Gordillo M, Sakai N, Yanagihara I, Yamada M, et al. Roberts syndrome is caused by mutations in ESCO2, a human homolog of yeast ECO1 that is essential for the establishment of sister chromatid cohesion. Nat Genet. 2005 May;37(5):468–70.

592 37. Musio A, Selicorni A, Focarelli ML, Gervasini C, Milani D, Russo S, et al. X-linked Cornelia
593 de Lange syndrome owing to SMC1L1 mutations. Nat Genet. 2006 May;38(5):528–30.

594 38. Deardorff MA, Kaur M, Yaeger D, Rampuria A, Korolev S, Pie J, et al. Mutations in Cohesin
595 Complex Members SMC3 and SMC1A Cause a Mild Variant of Cornelia de Lange
596 Syndrome with Predominant Mental Retardation. The American Journal of Human
597 Genetics. 2007 Mar;80(3):485–94.

598 39. Gordillo M, Vega H, Trainer AH, Hou F, Sakai N, Luque R, et al. The molecular mechanism
599 underlying Roberts syndrome involves loss of ESCO2 acetyltransferase activity. Human
600 Molecular Genetics. 2008 July 15;17(14):2172–80.

601 40. Antony J, Chin CV, Horsfield JA. Cohesin Mutations in Cancer: Emerging Therapeutic
602 Targets. Int J Mol Sci. 2021 June 24;22(13):6788.

603 41. Di Nardo M, Pallotta MM, Musio A. The multifaceted roles of cohesin in cancer. J Exp Clin
604 Cancer Res. 2022 Dec;41(1):96.

605 42. Pati D. Role of chromosomal cohesion and separation in aneuploidy and tumorigenesis.
606 Cell Mol Life Sci. 2024 Feb 22;81(1):100.

607 43. Yun J, Song SH, Kang JY, Park J, Kim HP, Han SW, et al. Reduced cohesin destabilizes
608 high-level gene amplification by disrupting pre-replication complex bindings in human
609 cancers with chromosomal instability. Nucleic Acids Res. 2016 Jan 29;44(2):558–72.

610 44. Xu H, Yan M, Patra J, Natrajan R, Yan Y, Swagemakers S, et al. Enhanced RAD21 cohesin
611 expression confers poor prognosis and resistance to chemotherapy in high grade luminal,
612 basal and HER2 breast cancers. Breast Cancer Res [Internet]. 2011 Jan 21 [cited 2025
613 July 15];13(1). Available from: https://breast-cancer-
614 research.biomedcentral.com/articles/10.1186/bcr2814

615 45. Sarogni P, Palumbo O, Servadio A, Astigiano S, D'Alessio B, Gatti V, et al. Overexpression
616 of the cohesin-core subunit SMC1A contributes to colorectal cancer development. J Exp
617 Clin Cancer Res [Internet]. 2019 Dec [cited 2025 July 15];38(1). Available from:
618 https://jeccr.biomedcentral.com/articles/10.1186/s13046-019-1116-0

619 46. Huang Y, Chen D, Bai Y, Zhang Y, Zheng Z, Fu Q, et al. ESCO2's oncogenic role in human
620 tumors: a pan-cancer analysis and experimental validation. BMC Cancer [Internet]. 2024
621 Apr 11 [cited 2025 July 16];24(1). Available from:
622 https://bmccancer.biomedcentral.com/articles/10.1186/s12885-024-12213-w

623 47. Gan W, Wang W, Li T, Zhang R, Hou Y, Lv S, et al. Prognostic Values and Underlying
624 Regulatory Network of Cohesin Subunits in Esophageal Carcinoma. J Cancer.
625 2022;13(5):1588–602.

626 48. Skibbens RV, Corson LB, Koshland D, Hieter P. Ctf7p is essential for sister chromatid
627 cohesion and links mitotic chromosome structure to the DNA replication machinery. Genes
628 & Development. 1999 Feb 1;13(3):307–19.

629 49. Tanaka K, Yonekawa T, Kawasaki Y, Kai M, Furuya K, Iwasaki M, et al. Fission Yeast
630 Eso1p Is Required for Establishing Sister Chromatid Cohesion during S Phase. Molecular
631 and Cellular Biology. 2000 May 1;20(10):3459–69.

632 50. Hoque MdT, Ishikawa F. Cohesin Defects Lead to Premature Sister Chromatid Separation,
633 Kinetochore Dysfunction, and Spindle-assembly Checkpoint Activation. Journal of
634 Biological Chemistry. 2002 Nov;277(44):42306–14.

635 51. Li X, Nicklas RB. Mitotic forces control a cell-cycle checkpoint. Nature. 1995
636 Feb;373(6515):630–2.

637 52. Nicklas RB. How Cells Get the Right Chromosomes. Science. 1997 Jan
638 31;275(5300):632–7.

639 53. Kuhn J, Dumont S. Mammalian kinetochores count attached microtubules in a sensitive
640 and switch-like manner. Journal of Cell Biology. 2019 Nov 4;218(11):3583–96.

641 54. Aist JR, Liang H, Berns MW. Astral and spindle forces in PtK2 cells during anaphase B: a
642 laser microbeam study. Journal of Cell Science. 1993 Apr 1;104(4):1207–16.

643 55. Rieder CL, Davison EA, Jensen LC, Cassimeris L, Salmon ED. Oscillatory movements of
644 monooriented chromosomes and their position relative to the spindle pole result from the
645 ejection properties of the aster and half-spindle. The Journal of cell biology. 1986 Aug
646 1;103(2):581–91.

647 56. Skibbens RV, Rieder CL, Salmon ED. Kinetochore motility after severing between sister
648 centromeres using laser microsurgery: Evidence that kinetochore directional instability and
649 position is regulated by tension. Journal of Cell Science. 1995 July 1;108(7):2537–48.

650 57. Kim ST, Xu B, Kastan MB. Involvement of the cohesin protein, Smc1, in Atm-dependent
651 and independent responses to DNA damage. Genes Dev. 2002 Mar 1;16(5):560–70.

652 58. Ünal E, Arbel-Eden A, Sattler U, Shroff R, Lichten M, Haber JE, et al. DNA Damage
653 Response Pathway Uses Histone Modification to Assemble a Double-Strand Break-
654 Specific Cohesin Domain. Molecular Cell. 2004 Dec;16(6):991–1002.

655 59. Ström L, Lindroos HB, Shirahige K, Sjögren C. Postreplicative Recruitment of Cohesin to
656 Double-Strand Breaks Is Required for DNA Repair. Molecular Cell. 2004 Dec;16(6):1003–
657 15.

658 60. Ström L, Karlsson C, Lindroos HB, Wedahl S, Katou Y, Shirahige K, et al. Postreplicative
659 Formation of Cohesion Is Required for Repair and Induced by a Single DNA Break.
660 Science. 2007 July 13;317(5835):242–5.

661 61. Kong X, Ball AR, Pham HX, Zeng W, Chen HY, Schmiesing JA, et al. Distinct Functions of
662 Human Cohesin-SA1 and Cohesin-SA2 in Double-Strand Break Repair. Molecular and
663 Cellular Biology. 2014 Feb 1;34(4):685–98.

664 62. Luo H, Li Y, Mu JJ, Zhang J, Tonaka T, Hamamori Y, et al. Regulation of Intra-S Phase
665 Checkpoint by Ionizing Radiation (IR)-dependent and IR-independent Phosphorylation of
666 SMC3. Journal of Biological Chemistry. 2008 July;283(28):19176–83.

667 63. Watrin E, Peters JM. The cohesin complex is required for the DNA damage-induced G2/M
668 checkpoint in mammalian cells. EMBO J. 2009 Sept 2;28(17):2625–35.

669 64. Choudhary K, Itzkovich Z, Alonso-Perez E, Bishara H, Dunn B, Sherlock G, et al. S.
670 cerevisiae Cells Can Grow without the Pds5 Cohesin Subunit. Winston FM, editor. mBio.
671 2022 Aug 30;13(4):e01420-22.

672 65. Singh G, Skibbens RV. Fdo1, Fkh1, Fkh2, and the Swi6-Mbp1 MBF complex regulate
673 Mcd1 levels to impact eco1 rad61 cell growth in Saccharomyces cerevisiae. Genetics.
674 2024 Oct 7;228(2):iyae128.

675 66. Toth A, Ciosk R, Uhlmann F, Galova M, Schleiffer A, Nasmyth K. Yeast Cohesin complex
676 requires a conserved protein, Eco1p(Ctf7), to establish cohesion between sister
677 chromatids during DNA replication. Genes & Development. 1999 Feb 1;13(3):320–33.

678 67. D'Ambrosio LM, Lavoie BD. Pds5 Prevents the PolySUMO-Dependent Separation of Sister
679 Chromatids. Current Biology. 2014 Feb;24(4):361–71.

680 68. Bellows AM. Human EFO1p exhibits acetyltransferase activity and is a unique combination
681 of linker histone and Ctf7p/Eco1p chromatid cohesion establishment domains. Nucleic
682 Acids Research. 2003 Nov 1;31(21):6334–43.

683 69. Zhang J, Shi X, Li Y, Kim BJ, Jia J, Huang Z, et al. Acetylation of Smc3 by Eco1 Is
684 Required for S Phase Sister Chromatid Cohesion in Both Human and Yeast. Molecular
685 Cell. 2008 July;31(1):143–51.

686 70. Ben-Shahar TR, Heeger S, Lehane C, East P, Flynn H, Skehel M, et al. Eco1-Dependent
687 Cohesin Acetylation During Establishment of Sister Chromatid Cohesion. Science. 2008
688 July 25;321(5888):563–6.

689 71. Ünal E, Heidinger-Pauli JM, Kim W, Guacci V, Onn I, Gygi SP, et al. A Molecular
690 Determinant for the Establishment of Sister Chromatid Cohesion. Science. 2008 July
691 25;321(5888):566–9.

692 72. Rowland BD, Roig MB, Nishino T, Kurze A, Uluocak P, Mishra A, et al. Building Sister
693 Chromatid Cohesion: Smc3 Acetylation Counteracts an Antiestablishment Activity.
694 Molecular Cell. 2009 Mar;33(6):763–74.

695 73. Sutani T, Kawaguchi T, Kanno R, Itoh T, Shirahige K. Budding Yeast Wpl1(Rad61)-Pds5
696 Complex Counteracts Sister Chromatid Cohesion-Establishing Reaction. Current Biology.
697 2009 Mar;19(6):492–7.

698 74. Maradeo ME, Skibbens RV. The Elg1-RFC Clamp-Loading Complex Performs a Role in
699 Sister Chromatid Cohesion. Hardwick KG, editor. PLoS ONE. 2009 Mar 5;4(3):e4707.

700 75. Zuilkoski CM, Skibbens RV. PCNA antagonizes cohesin-dependent roles in genomic
701 stability. Polymenis M, editor. PLoS ONE. 2020 Oct 19;15(10):e0235103.

702 76. Tong K, Skibbens RV. Cohesin without Cohesion: A Novel Role for Pds5 in Saccharomyces
703 cerevisiae. Lichten M, editor. PLoS ONE. 2014 June 25;9(6):e100470.

704 77. Buskirk S, Skibbens RV. G1-Cyclin2 (Cln2) promotes chromosome hypercondensation in
705 *eco1/ctf7 rad61* null cells during hyperthermic stress in *Saccharomyces cerevisiae*. Tyers
706 M, editor. G3 Genes|Genomes|Genetics. 2022 July 29;12(8):jkac157.

707 78. Lopez-Serra L, Lengronne A, Borges V, Kelly G, Uhlmann F. Budding Yeast Wapl Controls
708 Sister Chromatid Cohesion Maintenance and Chromosome Condensation. Current
709 Biology. 2013 Jan;23(1):64–9.

710 79. Bloom MS, Koshland D, Guacci V. Cohesin Function in Cohesion, Condensation, and DNA
711 Repair Is Regulated by Wpl1p via a Common Mechanism in Saccharomyces cerevisiae.
712 Genetics. 2018 Jan;208(1):111–24.

713 80. Ciosk R, Shirayama M, Shevchenko A, Tanaka T, Toth A, Shevchenko A, et al. Cohesin's
714 Binding to Chromosomes Depends on a Separate Complex Consisting of Scc2 and Scc4
715 Proteins. Molecular Cell. 2000 Feb;5(2):243–54.

716 81. Lengronne A, McIntyre J, Katou Y, Kanoh Y, Hopfner KP, Shirahige K, et al. Establishment
717 of Sister Chromatid Cohesion at the S. cerevisiae Replication Fork. Molecular Cell. 2006
718 Sept;23(6):787–99.

719 82. Kogut I, Wang J, Guacci V, Mistry RK, Megee PC. The Scc2/Scc4 cohesin loader
720 determines the distribution of cohesin on budding yeast chromosomes. Genes Dev. 2009
721 Oct 1;23(19):2345–57.

722 83. Lopez-Serra L, Kelly G, Patel H, Stewart A, Uhlmann F. The Scc2–Scc4 complex acts in
723 sister chromatid cohesion and transcriptional regulation by maintaining nucleosome-free
724 regions. Nat Genet. 2014 Oct;46(10):1147–51.

725 84. Ciosk R, Zachariae W, Michaelis C, Shevchenko A, Mann M, Nasmyth K. An ESP1/PDS1
726 Complex Regulates Loss of Sister Chromatid Cohesion at the Metaphase to Anaphase
727 Transition in Yeast. Cell. 1998 June;93(6):1067–76.

728 85. Yamamoto A. Pds1p is required for faithful execution of anaphase in the yeast,
729 Saccharomyces cerevisiae. The Journal of Cell Biology. 1996 Apr 1;133(1):85–97.

730 86. Uhlmann F, Lottspeich F, Nasmyth K. Sister-chromatid separation at anaphase onset is
731 promoted by cleavage of the cohesin subunit Scc1. Nature. 1999 July;400(6739):37–42.

732 87. Yang H, Ren Q, Zhang Z. Cleavage of Mcd1 by Caspase-like Protease Esp1 Promotes
733 Apoptosis in Budding Yeast. Fox T, editor. MBoC. 2008 May;19(5):2127–34.

734 88. Uhlmann F, Wernic D, Poupart MA, Koonin EV, Nasmyth K. Cleavage of Cohesin by the
735 CD Clan Protease Separin Triggers Anaphase in Yeast. Cell. 2000 Oct;103(3):375–86.

736 89. Leissing TM, Luh LM, Cromm PM. Structure driven compound optimization in targeted
737 protein degradation. Drug Discovery Today: Technologies. 2020 Dec;37:73–82.

738 90. Khago D, Fucci IJ, Byrd RA. The Role of Conformational Dynamics in the Recognition and
739 Regulation of Ubiquitination. Molecules. 2020 Dec 15;25(24):5933.

91. Blaszczak E, Pasquier E, Le Dez G, Odrzywolski A, Lazarewicz N, Brossard A, et al. Dissecting Ubiquitylation and DNA Damage Response Pathways in the Yeast Saccharomyces cerevisiae Using a Proteome-Wide Approach. Mol Cell Proteomics. 2024 Jan;23(1):100695.

92. Swaney DL, Beltrao P, Starita L, Guo A, Rush J, Fields S, et al. Global analysis of phosphorylation and ubiquitylation cross-talk in protein degradation. Nat Methods. 2013 July;10(7):676–82.

93. Litwin I, Nowicka M, Markowska K, Maciaszczyk-Dziubińska E, Tomaszewska P, Wysocki R, et al. ISW1a modulates cohesin distribution in centromeric and pericentromeric regions. Nucleic Acids Research. 2023 Sept 22;51(17):9101–21.

94. Yang X, Song M, Wang Y, Tan T, Tian Z, Zhai B, et al. The ubiquitin–proteasome system regulates meiotic chromosome organization. Proc Natl Acad Sci USA [Internet]. 2022 Apr 26 [cited 2025 July 14];119(17). Available from: https://pnas.org/doi/full/10.1073/pnas.2106902119

95. Newman JRS, Wolf E, Kim PS. A computationally directed screen identifying interacting coiled coils from *Saccharomyces cerevisiae*. Proc Natl Acad Sci USA. 2000 Nov 21;97(24):13203–8.

96. Costanzo M, VanderSluis B, Koch EN, Baryshnikova A, Pons C, Tan G, et al. A global genetic interaction network maps a wiring diagram of cellular function. Science [Internet]. 2016 Sept 23 [cited 2025 July 14];353(6306). Available from: https://www.science.org/doi/10.1126/science.aaf1420

97. Zhang W, Yeung CHL, Wu L, Yuen KWY. E3 ubiquitin ligase Bre1 couples sister chromatid cohesion establishment to DNA replication in Saccharomyces cerevisiae. eLife. 2017 Oct 23;6:e28231.

98. Collins GA, Gomez TA, Deshaies RJ, Tansey WP. Combined chemical and genetic approach to inhibit proteolysis by the proteasome. Yeast. 2010 Nov;27(11):965–74.

99. Zhang J, Shi D, Li X, Ding L, Tang J, Liu C, et al. Rtt101-Mms1-Mms22 coordinates replication-coupled sister chromatid cohesion and nucleosome assembly. EMBO Reports. 2017 Aug;18(8):1294–305.

100. Duke G, Skibbens RV. Analysis of combinatorial cohesin subunit gene deletions in budding yeast. Surtees J, editor. GENETICS. 2025 Aug 6;230(4):iyaf107.

101. Eng T, Guacci V, Koshland D. Interallelic complementation provides functional evidence for cohesin–cohesin interactions on DNA. Bloom KS, editor. MBoC. 2015 Nov 15;26(23):4224–35.

102. Tong K, Skibbens RV. Pds5 regulators segregate cohesion and condensation pathways in *Saccharomyces cerevisiae*. Proc Natl Acad Sci USA. 2015 June 2;112(22):7021–6.

103. Mayer ML, Gygi SP, Aebersold R, Hieter P. Identification of RFC(Ctf18p, Ctf8p, Dcc1p). Molecular Cell. 2001 May;7(5):959–70.

104. D'Ambrosio C, Kelly G, Shirahige K, Uhlmann F. Condensin-Dependent rDNA Decatenation Introduces a Temporal Pattern to Chromosome Segregation. Current Biology. 2008 July;18(14):1084–9.

105. Guacci V, Hogan E, Koshland D. Chromosome condensation and sister chromatid pairing in budding yeast. The Journal of cell biology. 1994 May 1;125(3):517–30.

106. Orgil O, Matityahu A, Eng T, Guacci V, Koshland D, Onn I. A Conserved Domain in the Scc3 Subunit of Cohesin Mediates the Interaction with Both Mcd1 and the Cohesin Loader Complex. Jessberger R, editor. PLoS Genet. 2015 Mar 6;11(3):e1005036.

107. Woodman J, Hoffman M, Dzieciatkowska M, Hansen KC, Megee PC. Phosphorylation of the Scc2 cohesin deposition complex subunit regulates chromosome condensation through cohesin integrity. Mol Biol Cell. 2015 Nov 1;26(21):3754–67.

108. Guacci V, Koshland D. Cohesin-independent segregation of sister chromatids in budding yeast. Cohen-Fix O, editor. MBoC. 2012 Feb 15;23(4):729–39.

109. Maradeo ME, Skibbens RV. Replication Factor C Complexes Play Unique Pro- and Anti-Establishment Roles in Sister Chromatid Cohesion. Lichten M, editor. PLoS ONE. 2010 Oct 27;5(10):e15381.

110. Kim JS, He X, Orr B, Wutz G, Hill V, Peters JM, et al. Intact Cohesion, Anaphase, and Chromosome Segregation in Human Cells Harboring Tumor-Derived Mutations in STAG2. Sullivan BA, editor. PLoS Genet. 2016 Feb 12;12(2):e1005865.

111. Adane B, Alexe G, Seong BKA, Lu D, Hwang EE, Hnisz D, et al. STAG2 loss rewires oncogenic and developmental programs to promote metastasis in Ewing sarcoma. Cancer Cell. 2021 June;39(6):827-844.e10.

112. Arruda NL, Carico ZM, Justice M, Liu YF, Zhou J, Stefan HC, et al. Distinct and overlapping roles of STAG1 and STAG2 in cohesin localization and gene expression in embryonic stem cells. Epigenetics & Chromatin. 2020 Dec;13(1):32.

113. Oreskovic E, Wheeler EC, Mengwasser KE, Fujimura E, Martin TD, Tothova Z, et al. Genetic analysis of cancer drivers reveals cohesin and CTCF as suppressors of PD-L1. Proc Natl Acad Sci USA. 2022 Feb 15;119(7):e2120540119.

114. Giménez-Llorente D, Cuadrado A, Andreu MJ, Sanclemente-Alamán I, Solé-Ferran M, Rodríguez-Corsino M, et al. STAG2 loss in Ewing sarcoma alters enhancer-promoter contacts dependent and independent of EWS::FLI1. EMBO Rep. 2024 Nov 1;25(12):5537–60.

115. Yamamoto A. Pds1p is required for faithful execution of anaphase in the yeast, Saccharomyces cerevisiae. The Journal of Cell Biology. 1996 Apr 1;133(1):85–97.

116. Ciosk R, Zachariae W, Michaelis C, Shevchenko A, Mann M, Nasmyth K. An ESP1/PDS1 Complex Regulates Loss of Sister Chromatid Cohesion at the Metaphase to Anaphase Transition in Yeast. Cell. 1998 June;93(6):1067–76.

117. Cohen-Fix O, Peters JM, Kirschner MW, Koshland D. Anaphase initiation in Saccharomyces cerevisiae is controlled by the APC-dependent degradation of the anaphase inhibitor Pds1p. Genes Dev. 1996 Dec 15;10(24):3081–93.

118. Yang H, Ren Q, Zhang Z. Cleavage of Mcd1 by Caspase-like Protease Esp1 Promotes Apoptosis in Budding Yeast. Fox T, editor. MBoC. 2008 May;19(5):2127–34.

119. Ren Q, Liou LC, Gao Q, Bao X, Zhang Z. Bir1 Deletion Causes Malfunction of the Spindle Assembly Checkpoint and Apoptosis in Yeast. Front Oncol [Internet]. 2012 [cited 2025 July 15];2. Available from: http://journal.frontiersin.org/article/10.3389/fonc.2012.00093/abstract

120. Varshavsky A. The Ubiquitin System, Autophagy, and Regulated Protein Degradation. Annu Rev Biochem. 2017 June 20;86:123–8.

121. Livneh I, Kravtsova-Ivantsiv Y, Braten O, Kwon YT, Ciechanover A. Monoubiquitination joins polyubiquitination as an esteemed proteasomal targeting signal. Bioessays. 2017 June;39(6).

122. Chen F, Kamradt M, Mulcahy M, Byun Y, Xu H, McKay MJ, et al. Caspase Proteolysis of the Cohesin Component RAD21 Promotes Apoptosis. Journal of Biological Chemistry. 2002 May;277(19):16775–81.

123. Pati D, Zhang N, Plon SE. Linking Sister Chromatid Cohesion and Apoptosis: Role of Rad21. Molecular and Cellular Biology. 2002 Dec 1;22(23):8267–77.

124. Xu X, Wang D, Xu W, Li H, Chen N, Li N, et al. NIPBL-mediated RAD21 facilitates tumorigenicity by the PI3K pathway in non-small-cell lung cancer. Commun Biol. 2024 Feb 20;7(1):206.

125. Su XA, Stopsack KH, Schmidt DR, Ma D, Li Z, Scheet PA, et al. *RAD21* promotes oncogenesis and lethal progression of prostate cancer. Proc Natl Acad Sci USA. 2024 Sept 3;121(36):e2405543121.

126. Gou R, Li X, Dong H, Hu Y, Liu O, Liu J, et al. RAD21 Confers Poor Prognosis and Affects Ovarian Cancer Sensitivity to Poly(ADP-Ribose)Polymerase Inhibitors Through DNA Damage Repair. Front Oncol. 2022 July 4;12:936550.

127. Mahmood SF, Gruel N, Chapeaublanc E, Lescure A, Jones T, Reyal F, et al. A siRNA screen identifies RAD21 , EIF3H , CHRAC1 and TANC2 as driver genes within the 8q23, 8q24.3 and 17q23 amplicons in breast cancer with effects on cell growth, survival and transformation. Carcinogenesis. 2014 Mar;35(3):670–82.

128. Yamamoto G, Irie T, Aida T, Nagoshi Y, Tsuchiya R, Tachikawa T. Correlation of invasion and metastasis of cancer cells, and expression of the RAD21 gene in oral squamous cell carcinoma. Virchows Arch. 2006 Apr;448(4):435–41.

129. Supernat A, Łapińska-Szumczyk S, Sawicki S, Wydra D, Biernat W, Żaczek AJ. Deregulation of RAD21 and RUNX1 expression in endometrial cancer. Oncology Letters. 2012 Oct;4(4):727–32.

130. Atienza JM, Roth RB, Rosette C, Smylie KJ, Kammerer S, Rehbock J, et al. Suppression of *RAD21* gene expression decreases cell growth and enhances cytotoxicity of etoposide and bleomycin in human breast cancer cells. Molecular Cancer Therapeutics. 2005 Mar 1;4(3):361–8.

131. Xia L, Wang M, Li H, Tang X, Chen F, Cui J. The effect of aberrant expression and genetic polymorphisms of Rad21 on cervical cancer biology. Cancer Medicine. 2018 July;7(7):3393–405.

132. Rose MD, Winston F, Hieter P. Methods in yeast genetics. New York: Cold Spring Harbor Laboratory Press; 1990.

133. Longtine MS, Mckenzie Iii A, Demarini DJ, Shah NG, Wach A, Brachat A, et al. Additional modules for versatile and economical PCR-based gene deletion and modification in Saccharomyces cerevisiae. Yeast. 1998 Dec 4;14(10):953–61.

134. Kenna MA, Skibbens RV. Mechanical Link between Cohesion Establishment and DNA Replication: Ctf7p/Eco1p, a Cohesion Establishment Factor, Associates with Three Different Replication Factor C Complexes. Molecular and Cellular Biology. 2003 Apr 1;23(8):2999–3007.

135. Foiani M, Marini F, Gamba D, Lucchini G, Plevani P. The B Subunit of the DNA Polymerase α-Primase Complex in *Saccharomyces cerevisiae* Executes an Essential Function at the Initial Stage of DNA Replication. Molecular and Cellular Biology. 1994 Feb 1;14(2):923–33.

136. Livak KJ, Schmittgen TD. Analysis of Relative Gene Expression Data Using Real-Time Quantitative PCR and the 2−ΔΔCT Method. Methods. 2001 Dec;25(4):402–8.

## FIGURE LEGENDS

**Fig 1. Mcd1 protein levels are reduced in *eco1-203* and *rad61*Δ mutated cells.** (A) Flow cytometry data of DNA contents for wildtype (YPH499), *eco1-203* (YBS514), *rad61*Δ (YMM808) and *eco1*Δ *rad61*Δ (YBS829) mutant cells. Log phase cultures were synchronized in S phase at their respective permissive temperatures, 23°C for *eco1-203* and 30°C for wildtype *eco1*Δ *rad61*Δ and *rad61*Δ mutant cells, then shifted to 37°C for 1 hr. (B) Representative Western Blot of Mcd1 (top panel) and Pgk1 (lower panel) protein obtained from extracts of HU-synchronized wildtype, *eco1-203*, *rad61*Δ and *eco1*Δ *rad61*Δ mutant cells indicated in (A). * indicates non-specific band. (C) Quantification of Mcd1, normalized to Pgk1 loading controls. Statistical analysis was performed using a two-tailed *t*-test. Statistical differences (*) are based

885 on a $P < 0.05$ obtained across three experiments (n=3). Error bars indicate the standard
886 deviation.
887
888 **Fig 2. Mcd1 protein levels are reduced in *scc2-4* mutated cells.** (A) Flow cytometry
889 data of DNA content for log phase of wildtype (YBS2031/KT046) and *scc2-4* cells
890 (YBS2033/KT048) arrested in S phase at 23°C for 2 hours and shifted to 37°C for 1 hour. (B)
891 Western Blot of Mcd1 (top panel) and Pgk1 (lower panel) protein obtained from extracts of HU-
892 synchronized cells indicated in (A). * indicates non-specific band. (C) Quantification of Mcd1,
893 normalized to Pgk1 loading controls. Statistical analysis was performed using a two-tailed *t*-test.
894 Statistical differences (*) are based on a $P < 0.05$ obtained across three experiments (n=3).
895 Error bars indicate the standard deviation.
896
897 **Fig 3. *MCD1* mRNA expression is increased in *eco1*Δ *rad61*Δ double mutant cells.**
898 (A) Flow cytometry data of DNA content for log phase wildtype (YPH499) and *eco1*Δ *rad61*Δ
899 (YBS829) double mutant cells arrested in S phase at 30°C for 3 hrs. (B) Representative
900 Western Blot of Mcd1 (top panel) and Pgk1 (lower panel) protein obtained from extracts of HU-
901 synchronized wildtype and *eco1*Δ *rad61*Δ double mutant cells indicated in (A). (C) Quantification
902 of Mcd1, normalized to Pgk1 loading controls. Statistical analysis was performed using a two-
903 tailed *t*-test. Statistical differences (**) are based on a $P < 0.01$ obtained across four
904 experiments (n=4). Error bars indicate the standard deviation. (D) Quantification of *MCD1*
905 mRNA fold change normalized to the expression of the housekeeping gene *ALG9*. Statistical
906 analysis was performed using a two-tailed *t*-test. Statistical differences (*) are based on a $P <$
907 $0.05$ obtained across four experiments (n=4). Error bars indicate the standard deviation.
908
909 **Fig 4. Deletion of Ubiquitin E3 ligases *SAN1* and *DAS1* suppress the growth**
910 **defects of *eco1*Δ *rad61*Δ double mutant cells.** (A) Growth of 10-fold serial dilutions of

911 wildtype (YPH499), *bul2*Δ (YGS277), *eco1*Δ *rad61*Δ (YBS829) and two independent isolates of
912 *eco1*Δ *rad61*Δ *bul2*Δ triple mutant cells (YGS279, YGS280); (B) wildtype (YPH499), *bre1*Δ
913 (YGS309), *eco1*Δ *rad61*Δ (YBS829) and two independent isolates of *eco1*Δ *rad61*Δ *bre1*Δ triple
914 mutant cells (YGS292, YGS293); (C) wildtype (YPH499), *ldb19*Δ (YGS281), *eco1*Δ *rad61*Δ
915 (YBS829) and two independent isolates of *eco1*Δ *rad61*Δ *ldb19*Δ triple mutant cells (YGS282,
916 YGS283); (D) wildtype (YPH499), *ubr1*Δ (YGS352), *eco1*Δ *rad61*Δ (YBS828) and two
917 independent isolates of *eco1*Δ *rad61*Δ *ubr1*Δ triple mutant cells (YGS354, YGS355). (E)
918 wildtype (YPH499), *san1*Δ (YGS284), *eco1*Δ *rad61*Δ (YBS829) and two independent isolates of
919 *eco1*Δ *rad61*Δ *san1*Δ triple mutant cells (YGS286, YGS287); and (F) wildtype (YPH499), *das1*Δ
920 (YGS288), *eco1*Δ *rad61*Δ (YBS829) and two independent isolates of *eco1*Δ *rad61*Δ *das1*Δ triple
921 mutant cells (YGS290, YGS291). Temperature and days of growth are indicated.
922
923 **Fig 5. San1 promotes Mcd1 degradation in the *eco1*Δ *rad61*Δ double mutant cells.**
924 (A) Flow cytometry data of DNA content for log phase of *eco1*Δ *rad61*Δ (YBS829) double mutant
925 cells and 3 biological replicates of *eco1*Δ *rad61*Δ *san1*Δ (YGS290) arrested in S phase at 30°C
926 for 3 hrs. (B) Western Blot of Mcd1 (top panel) and Pgk1 (lower panel) protein obtained from
927 extracts of HU-synchronized cells indicated in (A). * indicates non-specific band. (C)
928 Quantification of Mcd1, normalized to Pgk1 loading controls. Statistical analysis was performed
929 using a one sample t-test, two tailed. Statistical differences (**) are based on a $P \leq 0.01$
930 obtained across three biological replicates (n=3). Error bars indicate the standard deviation.
931
932 **Fig 6. Addition of MG-132 in M phase arrested cells elevates Mcd1 levels.** (A) Flow
933 cytometry data of DNA content for log phase of *eco1*Δ *rad61*Δ *pdr5*Δ cells (YGS377) arrested in
934 M phase with nocodazole at 30°C for 3 hours in the presence of DMSO (control) or MG-132
935 proteosome inhibitor. (B) Representative western Blot of Mcd1 (top panel) and Pgk1 (lower
936 panel) protein obtained from extracts of M phase synchronized cells indicated in (A). * indicates

937 non-specific band. (C) Quantification of Mcd1, normalized to Pgk1 loading controls. Statistical
938 analysis was performed using a two-tailed *t*-test. Statistical differences (*) are based on a $P <$
939 0.05 obtained across four experiments (n=4). Error bars indicate the standard deviation.
940
941 **Fig 7. Increased Mcd1 levels partially rescue the growth defects of cohesin**
942 **mutated cells.** Growth of 10-fold serial dilutions of cells (strains indicated below) that contains
943 either 2μ vector (pRS424) or 2μ vector that contains *MCD1* (pBS1476). Two independent
944 isolates are shown of mutated strains that express elevated levels of *MCD1*. Cell strains are as
945 follows for (A-E): wildtype (YGS209, YBS4558, YGS216), *smc3-42* (YGS229), *smc1-259*
946 (YGS211), *scc3-6* (YBS4568), *eco1*$^{ctf7}$*-203* (YGS329), and *scc2-4* (YGS218) all contain vector
947 alone. Wildtype (YGS210, YBS4562, YGS217), *smc3-42* (YGS230, YGS231), *smc1-259*
948 (YGS212, YGS213), *scc3-6* (YBS4569), *eco1*$^{ctf7}$*-203* (YGS330, YGS331), and *scc2-4* (YGS219,
949 YGS220) all contain elevated *MCD1* expression. Temperature and days of growth are indicated.
950 Strain genotypes are provided in S1 Table.
951
952 **Fig 8. Increased Mcd1 protein levels suppress *smc1-259* cell condensation**
953 **defects.** (A) Flow cytometry data of DNA content for log phase cells pre-synchronized in G1
954 phase at 23°C, then shifted to 34°C (the non-permissive temperature of *smc1-259*) in
955 nocodazole. Genotypes of wildtype (YGS335, YGS337) and *smc1-259* mutated (YGS338,
956 YGS341) cells that contain either 2μ vector (pRS424) or 2μ vector that contains *MCD1* are
957 provided in S1 Table. (B) Representative micrographs of rDNA detected by Net1-GFP. DNA is
958 detected by DAPI staining. (C) The percentage of cells with condensed rDNA is plotted. At least
959 120 nuclei were scored per genotype. Statistical analysis was performed using a two-tailed *t*-
960 test. Statistical differences (**) are based on a $P < 0.01$ obtained across two experiments (n=2).
961 ns indicates not significantly different. Error bars indicate the standard deviation. (D) The
962 uncondensed rDNA structures for all strains were further classified as either fully decondensed

963 “puffs” or partially decondensed “partial”. Statistical analysis was performed using a two-tailed *t*-
964 test. Statistical differences (**) are based on a $P < 0.01$, and (***) are based on a $P < 0.001$
965 obtained across two experiments (n=2). Error bars indicate the standard deviation.
966
967 **Fig 9. Increased Mcd1 levels significantly suppress sister chromatid cohesion**
968 **defects in *smc1-259* cells.** (A) Flow cytometry data of DNA content as described in Fig 8. (B)
969 Representative micrographs of GFP dots (markers of sister chromatid cohesion) in cell
970 treatments as described in Fig 8. Genotypes of wildtype (YGS333, YGS334) and *smc1-259*
971 mutated (YGS321, YGS323) cells modified to contain both cohesion cassettes and either 2μ
972 vector (pRS424) or 2μ vector that contains *MCD1* are provided in S1 Table. (C) The percentage
973 of cells in which sisters are separated (two GFP spots indicated of a sister chromatid cohesion
974 defect) is plotted. At least 120 cells were scored for each genotype. Statistical analysis was
975 performed using a two-tailed *t*-test. Statistical differences (ns) are based on a $P > 0.05$, (*) are
976 based on a $P < 0.05$ and (**) are based on a $P < 0.01$ obtained across two experiments (n=2).
977 Error bars indicate the standard deviation.
978
979 **S1 Fig. Pds5 protein levels are maintained in the *eco1*Δ *rad61*Δ mutated cells, and**
980 ***PDS5* overexpression does not rescue *eco1*Δ *rad61*Δ cells growth defects.** (A) Flow
981 cytometry data of DNA content for log phase wildtype (YPH499) and *eco1*Δ *rad61*Δ (YBS828)
982 double mutant cells arrested in S phase at 30°C for 3 hrs. (B) Representative Western Blot of
983 Mcd1 (top panel) and Pds5 (middle) and Pgk1 (lower panel) protein obtained from extracts of
984 HU-synchronized wildtype and *eco1*Δ *rad61*Δ mutant cells indicated in (A). * indicates non-
985 specific band. (C) Quantification of Pds5, normalized to Pgk1 loading controls. Statistical
986 analysis was performed using a two-tailed *t*-test. Statistical differences (ns) are based on a $P >$
987 $0.05$ obtained across three experiments (n=3). Error bars indicate the standard deviation. (D)
988 Growth of 10-fold serial dilutions of wildtype cells overexpressing vector alone (YBS4067) or

989 overexpressing *PDS5* (YBS4071) and *eco1*Δ *rad61*Δ overexpressing vector alone (YBS4069) or
990 overexpressing *PDS5* (YBS4075, YBS4076).
991
992 **S2 Fig. Mutation of *ESP1* fails to suppress the growth defects of *eco1*Δ *rad61*Δ**
993 **double mutant cells.** (A) Schematic key for the following strains: wildtype (YPH499), *eco1*Δ
994 *rad61*Δ *esp1-1* (YBS4864*), esp1-1* (YBS4862, YBS4863), *eco1*Δ *rad61*Δ (YBS4860, YBS4861).
995 (B) Streak assay for the strains indicated in (A) at 23°C and 34°C.
996
997 **S3 Fig. Addition of MG-132 in S phase arrested cells fails to increase Mcd1 levels.**
998 (A) Flow cytometry data of DNA content for log phase of *eco1*Δ *rad61*Δ *pdr5*Δ arrested in S
999 phase at 30°C for 2 hours, then treated with DMSO (control) or MG-132 in the continued
1000 presence of HU for an additional 2 hours. (B) Western Blot of Mcd1 (top panel) and Pgk1 (lower
1001 panel) protein obtained from extracts of HU-synchronized cells in DMSO or MG132 indicated in
1002 (A). “A” and “B” indicate independent biological replicates (YGS375, YGS377). * indicates non-
1003 specific band. (C) Quantification of Mcd1, normalized to Pgk1 loading controls. Statistical
1004 analysis was performed using a two-tailed *t*-test. Statistical differences (ns) are based on a $P >$
1005 0.05 obtained across two biological replicates (n=2). Error bars indicate the standard deviation.
1006
1007 **S4 Fig. Zoomed-in micrographs showing the effects of *MCD1* overexpression on**
1008 **sister chromatid cohesion and rDNA condensation in *smc1-259* cells.** (A) Enlarged
1009 micrographs from Fig 8B. Top panel: wildtype cells overexpressing vector alone. Middle panel:
1010 *smc1-259* cells overexpressing vector alone. Bottom panel: *smc1-259* cells overexpressing
1011 *MCD1*. Yellow arrow indicates a condensed, puff, or partially condensed rDNA (see Fig 8
1012 legend). (B) Enlarged micrographs from Fig 9B. Top panel: wildtype cells overexpressing vector

1013 alone. Middle panel: *smc1-259* cells overexpressing vector alone. Bottom panel: *smc1-259* cells

1014 overexpressing *MCD1* (see Fig 9 legend).

1015

1016 **S1 Table. Strains used in this study.**

1017

1018 **S2 Table. Oligonucleotides used in this study.**

1019

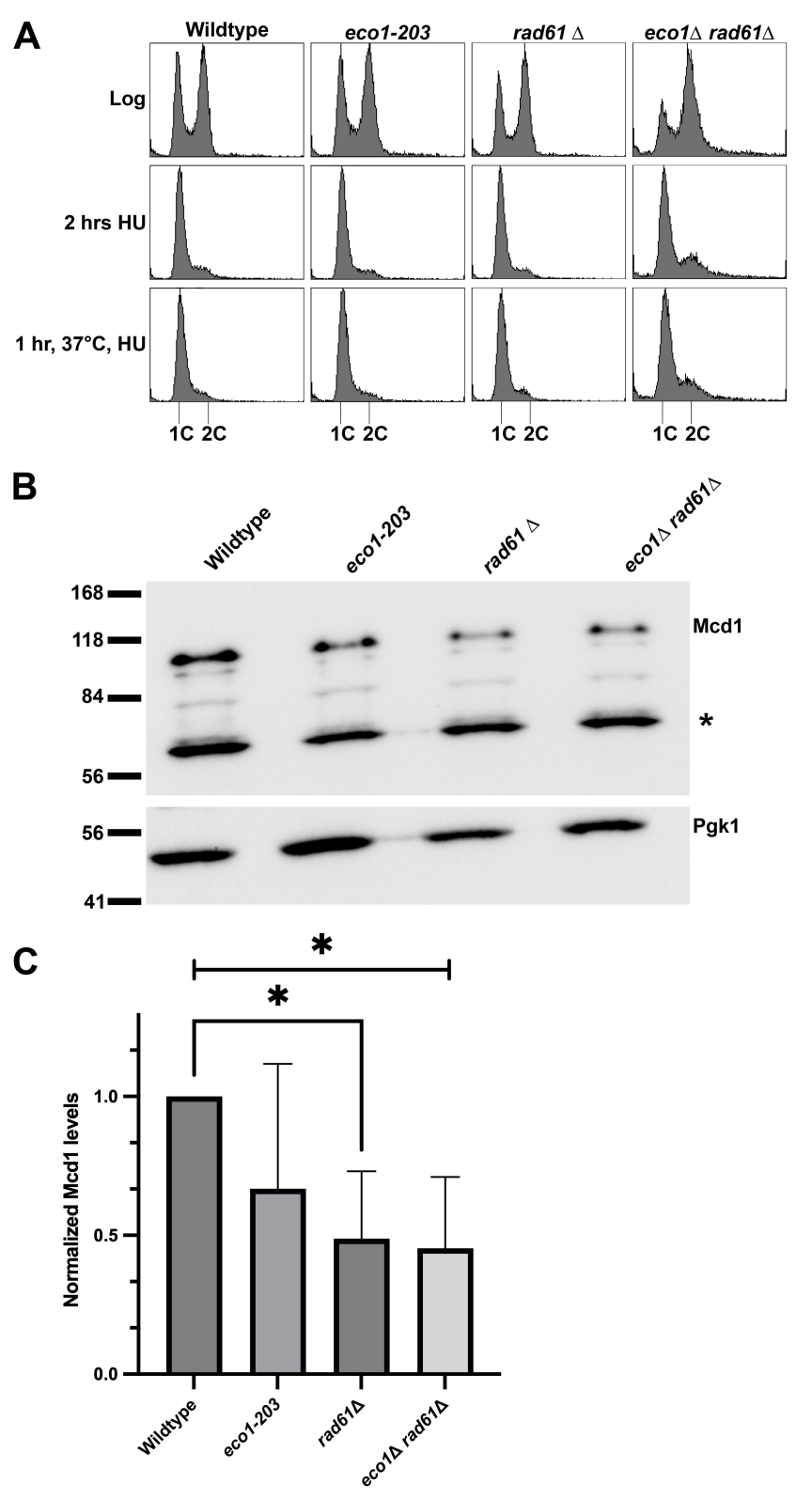
A
Wildtype
eco1-203
rad61 Δ
eco1Δ rad61Δ
Log
2 hrs HU
1 hr, 37°C, HU
1C 2C
1C 2C
1C 2C
1C 2C
B
Wildtype
eco1-203
rad61 Δ
eco1Δ rad61Δ
168
118
84
56
Mcd1
*
56
41
Pgk1
C
*
*
Normalized Mcd1 levels
1.0
0.5
0.0
Wildtype
eco1-203
rad61Δ
eco1Δ rad61Δ

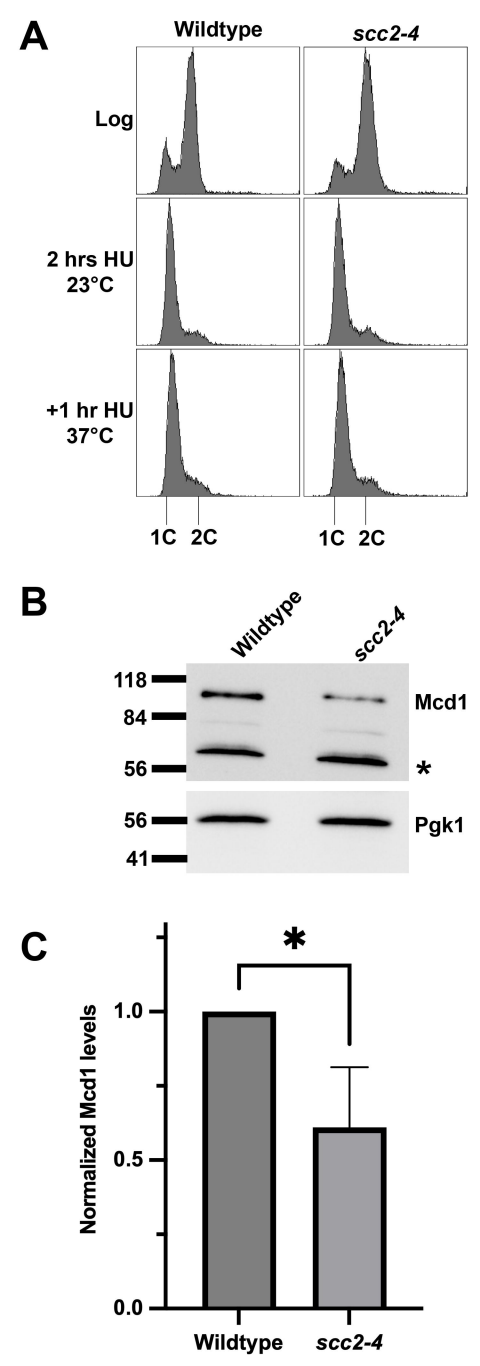
A
Wildtype
scc2-4
Log
2 hrs HU
23°C
+1 hr HU
37°C
1C
2C
1C
2C
B
Wildtype
scc2-4
118
84
56
Mcd1
*
56
41
Pgk1
C
*
Normalized Mcd1 levels
1.0
0.5
0.0
Wildtype
scc2-4

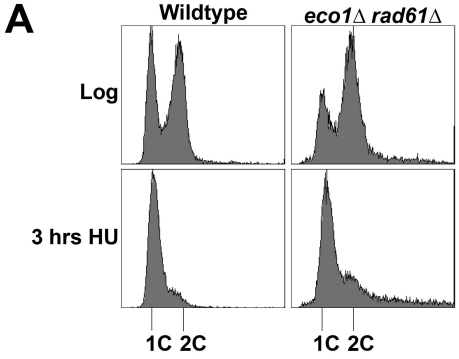
A
Wildtype
eco1Δ rad61Δ
Log
3 hrs HU
1C 2C
1C 2C

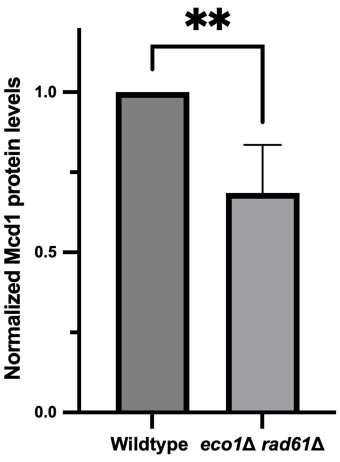
C
**
Normalized Mcd1 protein levels
1.0
0.5
0.0
Wildtype
eco1Δ rad61Δ

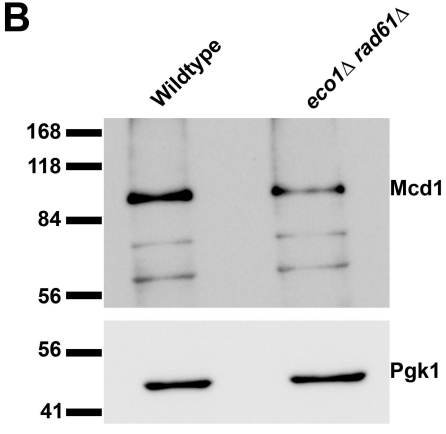
B
Wildtype
eco1Δ rad61Δ
168
118
84
56
Mcd1
56
41
Pgk1

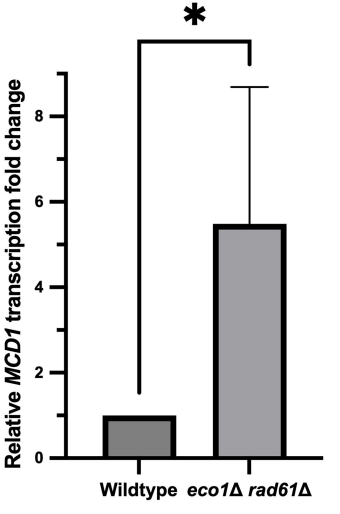
D
*
Relative MCD1 transcription fold change
8
6
4
2
0
Wildtype
eco1Δ rad61Δ

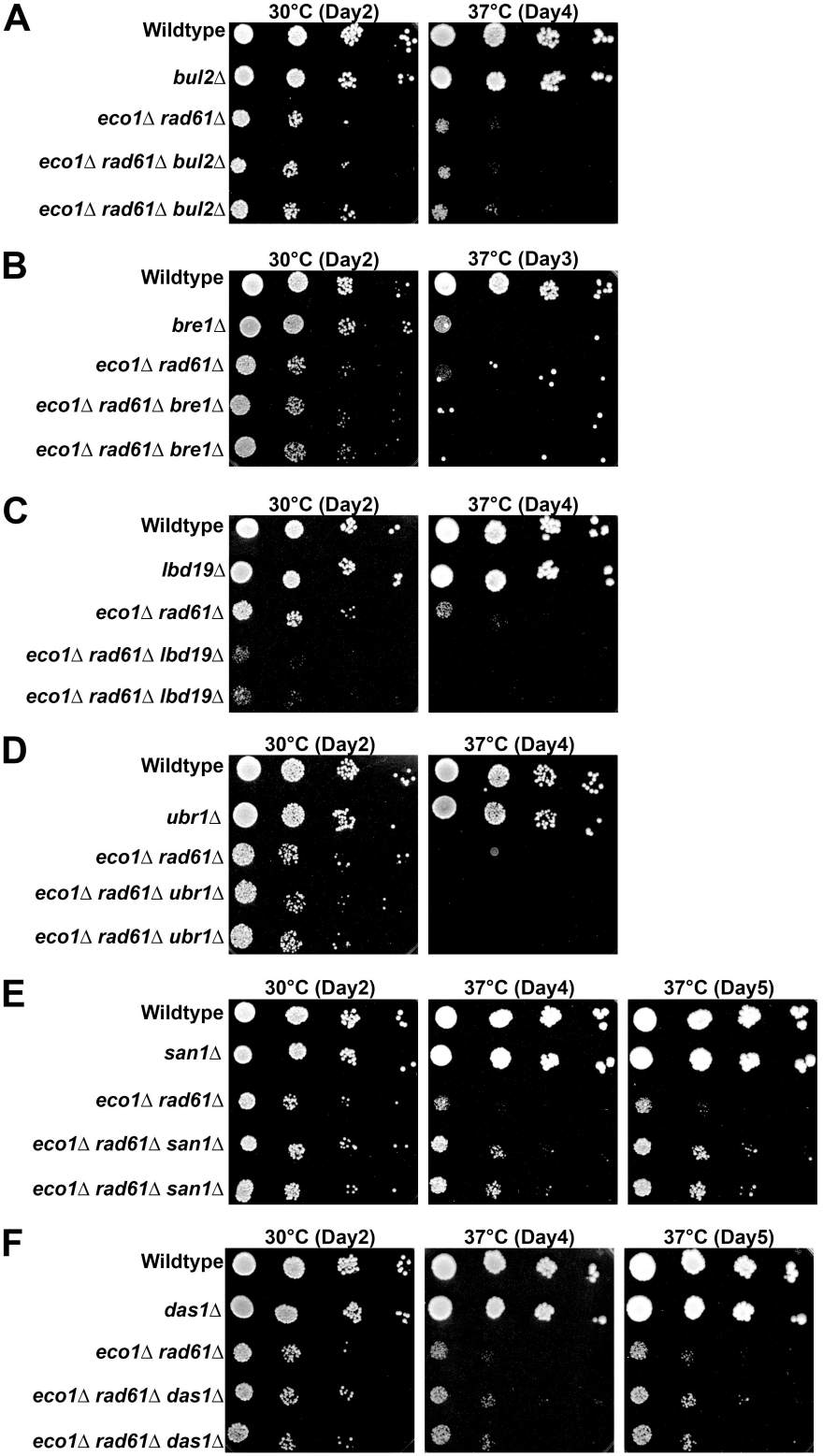
A
30°C (Day2)
37°C (Day4)
Wildtype
bul2Δ
eco1Δ rad61Δ
eco1Δ rad61Δ bul2Δ
eco1Δ rad61Δ bul2Δ
B
30°C (Day2)
37°C (Day3)
Wildtype
bre1Δ
eco1Δ rad61Δ
eco1Δ rad61Δ bre1Δ
eco1Δ rad61Δ bre1Δ
C
30°C (Day2)
37°C (Day4)
Wildtype
lbd19Δ
eco1Δ rad61Δ
eco1Δ rad61Δ lbd19Δ
eco1Δ rad61Δ lbd19Δ
D
30°C (Day2)
37°C (Day4)
Wildtype
ubr1Δ
eco1Δ rad61Δ
eco1Δ rad61Δ ubr1Δ
eco1Δ rad61Δ ubr1Δ
E
30°C (Day2)
37°C (Day4)
37°C (Day5)
Wildtype
san1Δ
eco1Δ rad61Δ
eco1Δ rad61Δ san1Δ
eco1Δ rad61Δ san1Δ
F
30°C (Day2)
37°C (Day4)
37°C (Day5)
Wildtype
das1Δ
eco1Δ rad61Δ
eco1Δ rad61Δ das1Δ
eco1Δ rad61Δ das1Δ

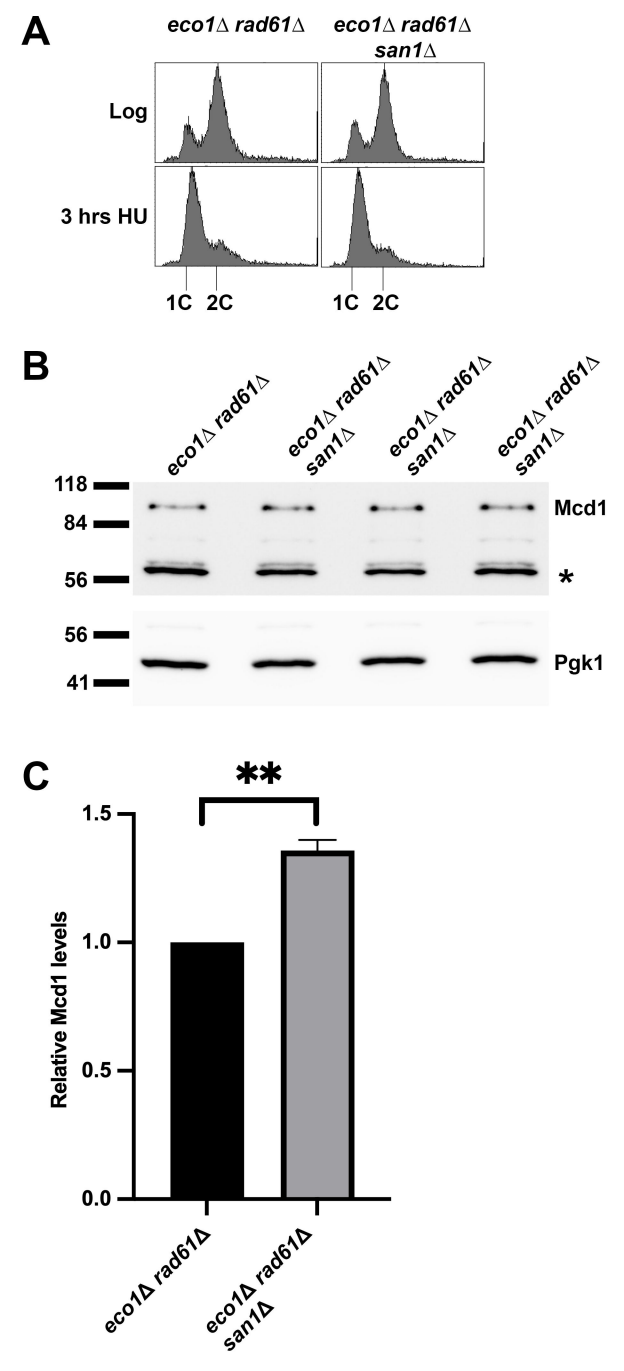
A
eco1Δ rad61Δ
eco1Δ rad61Δ san1Δ
Log
3 hrs HU
1C 2C
1C 2C
B
eco1Δ rad61Δ
eco1Δ rad61Δ san1Δ
eco1Δ rad61Δ san1Δ
eco1Δ rad61Δ san1Δ
118
84
56
Mcd1
*
56
41
Pgk1
C
**
1.5
1.0
0.5
0.0
Relative Mcd1 levels
eco1Δ rad61Δ
eco1Δ rad61Δ san1Δ

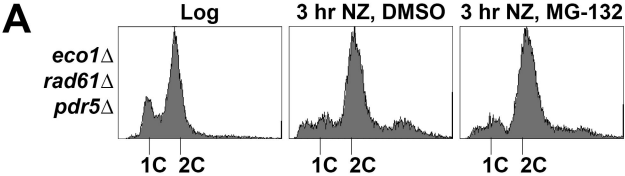
A
Log
3 hr NZ, DMSO
3 hr NZ, MG-132
eco1Δ
rad61Δ
pdr5Δ
1C 2C
1C 2C
1C 2C

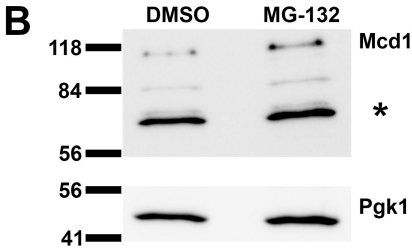
B
DMSO
MG-132
118
84
56
56
41
Mcd1
*
Pgk1

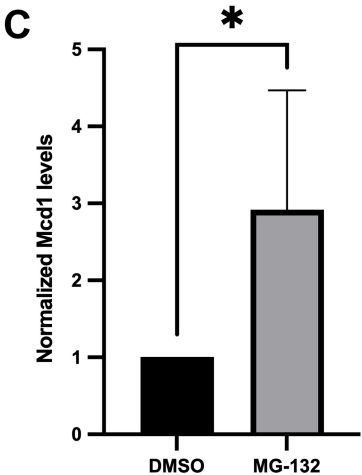
C
*
Normalized Mcd1 levels
0
1
2
3
4
5
DMSO
MG-132

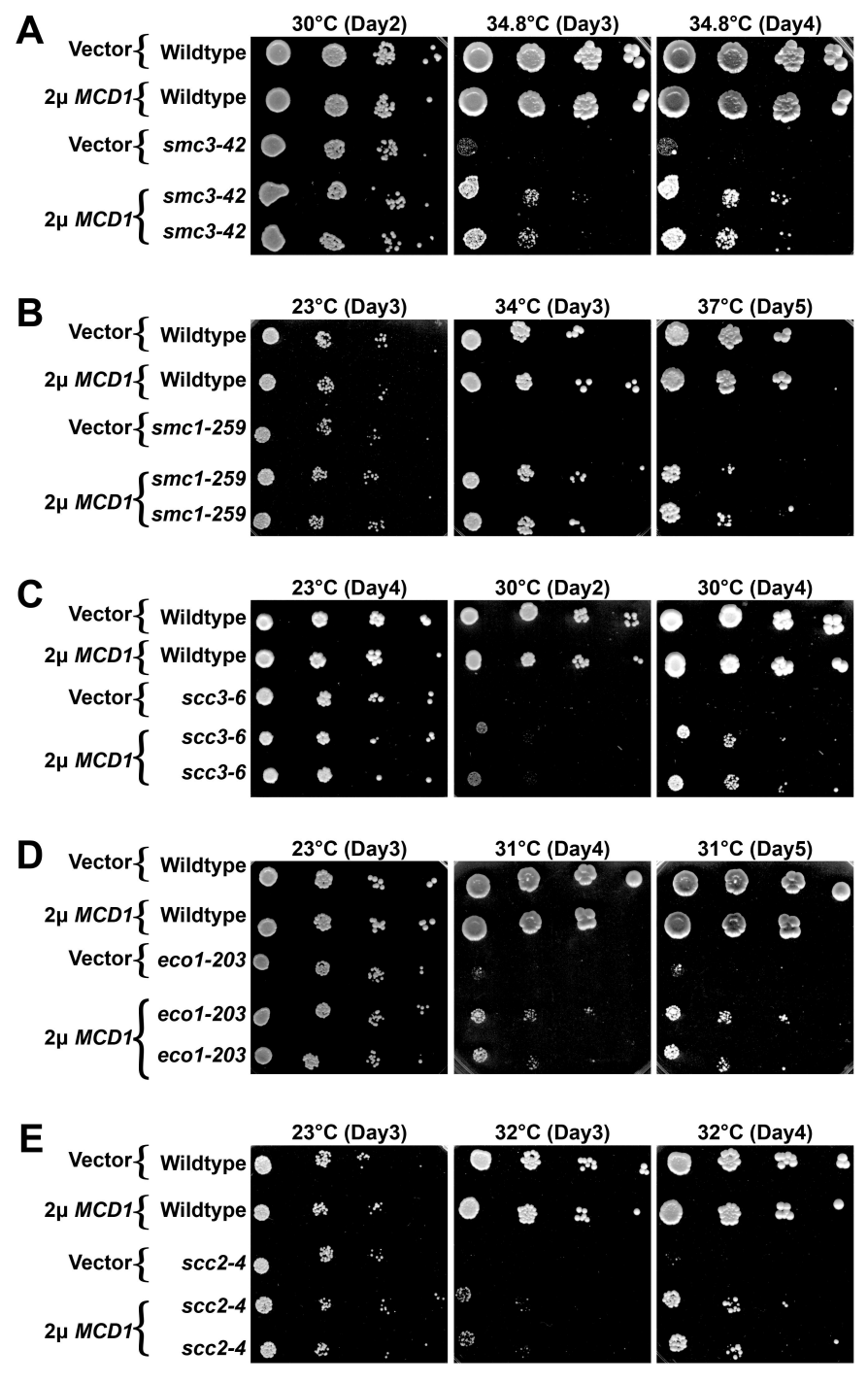
A
30°C (Day2)
34.8°C (Day3)
34.8°C (Day4)
Vector
Wildtype
2μ MCD1
Wildtype
Vector
smc3-42
2μ MCD1
smc3-42
smc3-42
B
23°C (Day3)
34°C (Day3)
37°C (Day5)
Vector
Wildtype
2μ MCD1
Wildtype
Vector
smc1-259
2μ MCD1
smc1-259
smc1-259
C
23°C (Day4)
30°C (Day2)
30°C (Day4)
Vector
Wildtype
2μ MCD1
Wildtype
Vector
scc3-6
2μ MCD1
scc3-6
scc3-6
D
23°C (Day3)
31°C (Day4)
31°C (Day5)
Vector
Wildtype
2μ MCD1
Wildtype
Vector
eco1-203
2μ MCD1
eco1-203
eco1-203
E
23°C (Day3)
32°C (Day3)
32°C (Day4)
Vector
Wildtype
2μ MCD1
Wildtype
Vector
scc2-4
2μ MCD1
scc2-4
scc2-4

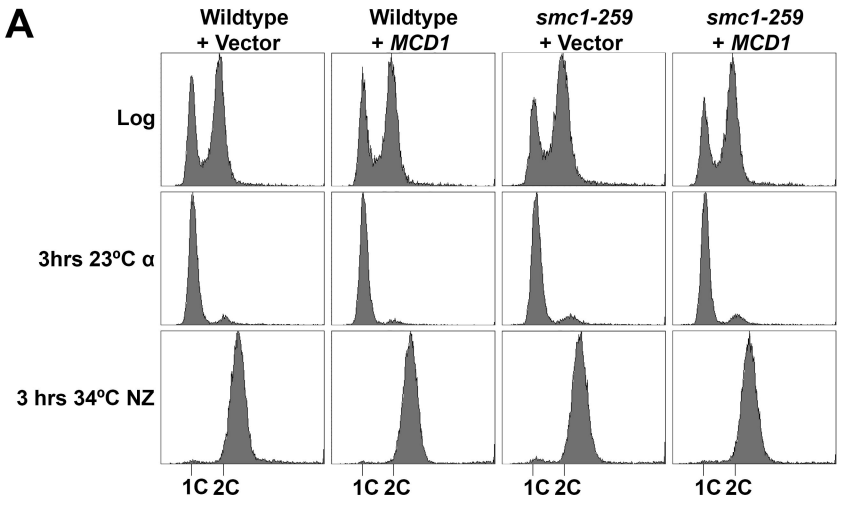
A
Wildtype + Vector
Wildtype + MCD1
smc1-259 + Vector
smc1-259 + MCD1
Log
3hrs 23ºC α
3 hrs 34ºC NZ
1C 2C
1C 2C
1C 2C
1C 2C

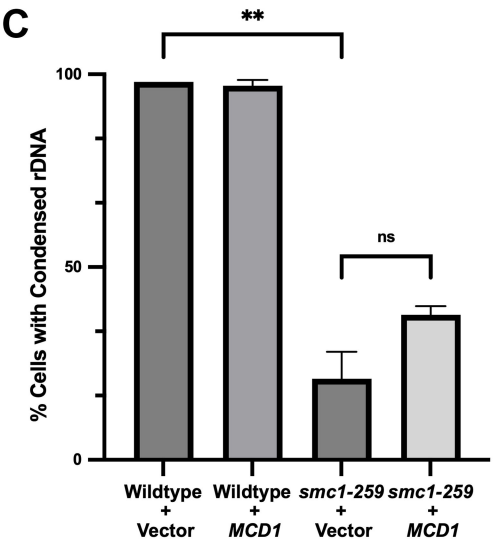
C
**
ns
100
50
0
% Cells with Condensed rDNA
Wildtype + Vector
Wildtype + MCD1
smc1-259 + Vector
smc1-259 + MCD1

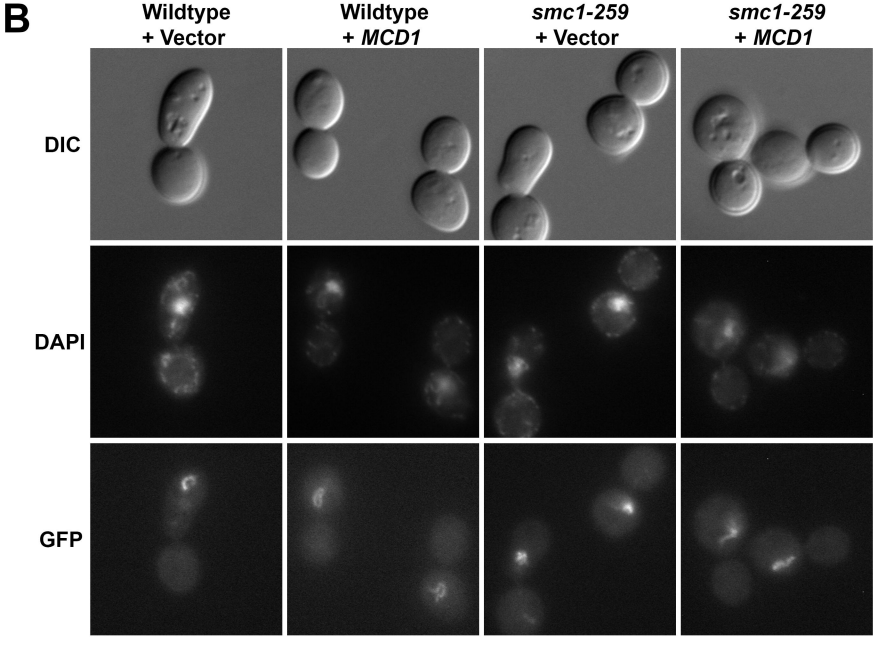
B
Wildtype + Vector
Wildtype + MCD1
smc1-259 + Vector
smc1-259 + MCD1
DIC
DAPI
GFP

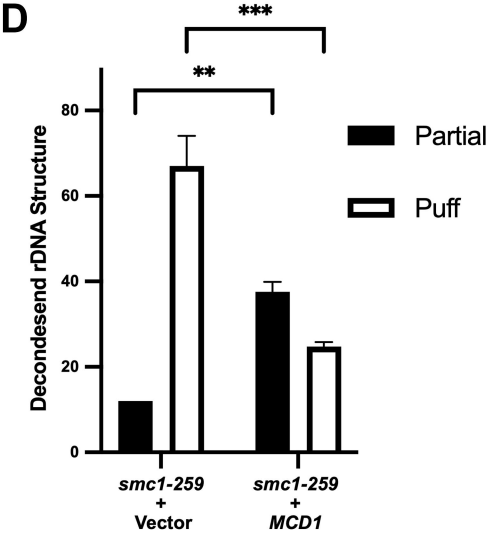
D
***
**
80
60
40
20
0
Decondesend rDNA Structure
Partial
Puff
smc1-259 + Vector
smc1-259 + MCD1

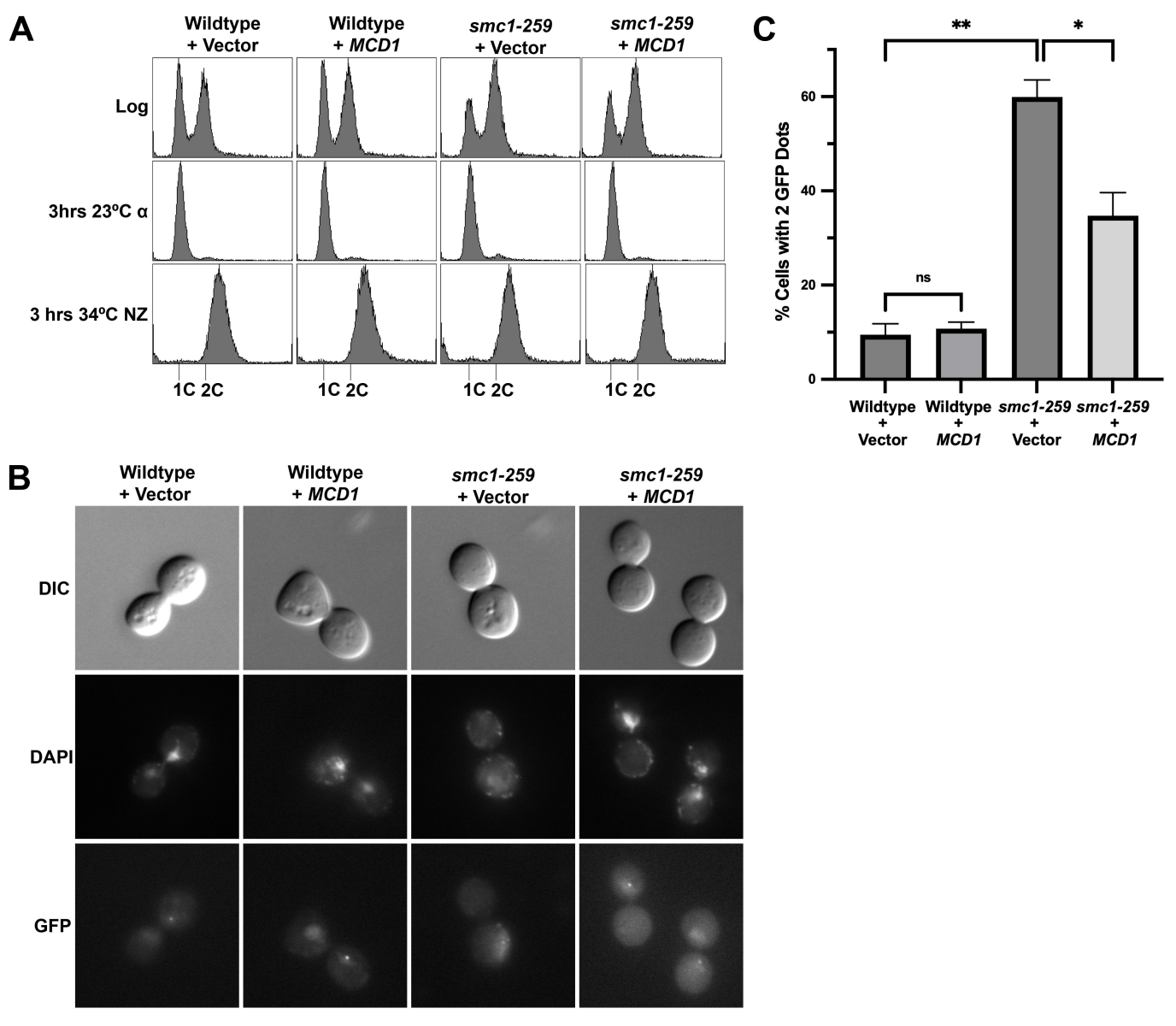
A
Wildtype + Vector
Wildtype + MCD1
smc1-259 + Vector
smc1-259 + MCD1
Log
3hrs 23ºC α
3 hrs 34ºC NZ
1C 2C
B
DIC
DAPI
GFP
C
% Cells with 2 GFP Dots
0
20
40
60
ns
**
*
Wildtype + Vector
Wildtype + MCD1
smc1-259 + Vector
smc1-259 + MCD1